Identification of Meibomian gland stem cell populations and mechanisms of aging

Xuming Zhu[1,2,3¶], Mingang Xu[1,2,3¶], Celine Portal[4,5], Yvonne Lin[4,5,^], Alyssa Ferdinand[1,2,3], Tien Peng[6], Edward E. Morrisey[7], Andrzej A. Dlugosz[8,9], Joseph M. Castellano[1,2,10,11], Vivian Lee[12,13], John T. Seykora[13], Carlo Iomini[4,5*], and Sarah E Millar[1,2,3,14,15*#]

[1]Black Family Stem Cell Institute, Icahn School of Medicine at Mount Sinai, New York, NY 10029, USA; [2]Institute for Regenerative Medicine, Icahn School of Medicine at Mount Sinai, New York, NY 10029, USA; [3]Department of Cell, Developmental and Regenerative Biology, Icahn School of Medicine at Mount Sinai, New York, NY 10029, USA; [4]Department of Ophthalmology, Wilmer Eye Institute, Johns Hopkins University School of Medicine, Baltimore, MD, 21231, USA; [5]Department of Cell Biology, Johns Hopkins University School of Medicine, Baltimore, MD, 21231, USA; [6]Department of Medicine, University of California San Francisco, San Francisco, CA 94143, USA; [7]Department of Medicine, Perelman School of Medicine at the University of Pennsylvania, Philadelphia, PA 19104, USA; [8]Department of Dermatology and the Rogel Cancer Center, University of Michigan Medical School, Ann Arbor, MI 48109, USA; [9]Department of Cell and Developmental Biology, University of Michigan Medical School, Ann Arbor, MI 48109, USA; [10]Nash Family Department of Neuroscience, Department of Neurology, Friedman Brain Institute, Icahn School of Medicine at Mount Sinai, New York, NY 10029, USA; [11]Ronald M. Loeb Center for Alzheimer's Disease, Icahn School of Medicine at Mount Sinai, New York, NY 10029, USA; [12]Department of Ophthalmology, Perelman School of Medicine at the University of Pennsylvania, Philadelphia, PA 19104, USA; [13]Department of Dermatology, Perelman School of Medicine at the University of Pennsylvania, Philadelphia, PA 19104, USA; [14]Department of Oncological Sciences, Icahn School of Medicine at Mount Sinai, New York, NY 10029, USA; [15]Tisch Cancer Institute, Icahn School of Medicine at Mount Sinai, New York, NY 10029, USA.

[¶]These authors contributed equally

^Current affiliation: Graduate School of Biomedical Sciences, Icahn School of Medicine at Mount Sinai, New York, NY 10029, USA.

*Co-corresponding authors: Carlo Iomini: ciomini1@jhmi.edu; Sarah E Millar: sarah.millar@mssm.edu

[#]Lead contact: Sarah E Millar: sarah.millar@mssm.edu

Summary

Meibomian glands secrete lipid-rich meibum, which prevents tear evaporation. Aging-related Meibomian gland shrinkage may result in part from stem cell exhaustion and is associated with evaporative dry eye disease, a common condition lacking effective treatment. The identities and niche of Meibomian gland stem cells and the signals controlling their activity are poorly defined. Using snRNA-seq, in vivo lineage tracing, ex vivo live imaging, and genetic studies in mice, we identified markers for stem cell populations that maintain distinct regions of the gland and uncovered Hh signaling as a key regulator of stem cell proliferation. Consistent with this, human Meibomian gland carcinoma exhibited increased Hh signaling. Aged glands displayed decreased Hh and EGF signaling, deficient innervation, and loss of collagen I in niche fibroblasts, indicating that alterations in both glandular epithelial cells and their surrounding microenvironment contribute to age-related degeneration. These findings suggest new approaches to treat aging-associated Meibomian gland loss.

Key words

Meibomian gland; stem cells; snRNA-seq; lineage tracing; live imaging; Hedgehog signaling; Smoothened; GLI2; EGF

Introduction

Meibomian glands (MGs) are specialized holocrine sebaceous glands (SGs) embedded in the tarsal plate of the upper and lower eyelids. These glands secrete lipid-rich meibum, which protects the eye surface by preventing tear film evaporation. In aging, MGs decrease in size and/or display reduced numbers of acini in humans and in mice, which provide a genetically manipulable model system for delineating molecular mechanisms controlling MG function. MG atrophy is associated with evaporative dry eye disease, a common condition in the aged population that can result in severe vision loss and currently has no effective therapy[1-3].

Each MG consists of multiple acini, which are connected to a central duct through short ductules. The MG central duct is a stratified squamous epithelial structure that includes basal and suprabasal layers[4,5]. In MG acini, basal cells proliferate toward the center of acinus, forming meibocytes which undergo sequential differentiation and accumulate lipid content. Upon reaching the center of acinus, fully differentiated meibocytes disintegrate and release meibum which reaches the ocular surface through an orifice in the eyelid margin via the ductule and central duct[4,5]. MGs develop independently of hair follicles (HFs) but share similarities with HF-associated SGs. Both types of glands secrete lipids in a holocrine manner and require constant replenishment of lipid-releasing cells from proliferating basal cells[4].

In addition to other proposed mechanisms, including duct hyper-keratinization, immune cell infiltration, and reduced acinar basal cell proliferation[6], MG dropout is thought to involve decreased activity of MG epithelial stem cells that normally maintain MGs by both self-renewing and yielding differentiating progeny[7,8,9-11]. However, the identities of MG stem cells, the nature of their supporting niche environment, and the mechanisms that control their functions in homeostasis and aging are poorly understood[12]. By contrast, single-cell analyses and lineage

tracing studies in mice have shown that *Lrig1*+ and *Lgr6*+ stem cells from the HF isthmus, which connects to the opening of the SG, contribute to homeostasis of the attached SGs[13-16]. Recent evidence suggests that the MG duct and acinus are separately maintained by distinct unipotent KRT14+ stem cells; however, KRT14 is ubiquitously expressed in the MG. MG ductules have also been proposed to harbor stem cells, based on the presence of label-retaining cells (LRCs) in ductules[12], but evidence that these LRCs directly contribute to MG homeostasis is lacking. Lineage tracing with a constitutive *Krox20/Egr2-Cre* mouse line shows that EGR2+ cells give rise to the MG during development. However, lineage tracing experiments with an inducible *Egr2-Cre* line to determine whether EGR2+ cells self-renew and give rise to differentiating progeny in adult MGs have not been performed. Thus, specific markers for adult MG stem cells have yet to be identified.

Stem cell activity is tightly regulated by intercellular signaling pathways[17,18]. These include the Hedgehog (Hh) pathway, which controls HF stem cell activity[19], regulates SG development[20], and promotes proliferation of undifferentiated human sebocytes in vitro[21]. Components of the Hh pathway are expressed in MGs[22], and Hh signaling controls the proliferation and differentiation of rat MG epithelial cells in vitro[23]; however, it is unknown whether Hh signaling regulates adult MG homeostasis and MG stem cell activity in vivo.

To begin to address these questions, we dissected tarsal plates from young and aged mice and performed single-nucleus RNA sequencing (snRNA-seq) to reveal the cell heterogeneity of adult mouse MGs and the changes in MG epithelial cells and the surrounding tissue niche that take place during aging. We used lineage tracing and ex vivo live imaging assays to test the contributions of cells expressing putative stem cell markers to MG homeostasis. These data identified multiple stem cell populations that can self-renew and produce differentiated progeny to maintain the MG duct and acinus. We found that loss of the Hh receptor Smoothened (SMO)

in MG epithelial cells caused decreased proliferation and MG dropout, while forced expression of an activated form of the Hh pathway effector GLI2 (GLI2ΔN) promoted expansion of MG stem cells at the expense of differentiated acini. GLI2 and other stem cell markers were expressed in human MG and showed elevated levels in MG carcinoma (MGC), suggesting that MGC involves expansion of MG stem cells. Aged versus young mouse MGs displayed fewer acinar basal cells and surrounding dermal cells expressing downstream Hh pathway genes. In parallel, aged MG exhibited lower levels of EGF signaling, decreased MG innervation, and dermal fibroblast dysfunction, identifying additional mechanisms that could contribute to MG degeneration in aging. In summary, our data uncover stem cell populations and molecular mechanisms that sustain the adult MG and are altered in aging and in human disease.

Results

snRNA-seq identifies multiple distinct populations of MG epithelial cells

The eyelid is a complex environment, containing epidermal, HF, and conjunctival cells closely adjacent to the MGs, making it challenging to isolate pure MG cells or to identify MG contributions in bulk RNA-seq analyses. To analyze transcription in MG subpopulations, and to overcome difficulties in isolating cytoplasmic mRNAs from lipid-rich acinar cells, we utilized snRNA-seq which allows for identification of cell sub-populations within a complex mix. Nuclei were analyzed from the pooled tarsal plates of four 8-week-old and four 21-month-old male mice using two replicates for each age (16 mice analyzed in total). UMAP analysis identified 34 clusters of tarsal plate cell populations (Figure 1A; Figure S1A) and confirmed similar cluster distributions between the four datasets and two conditions (Figure S1B, C, D). Cell populations were annotated based on their expression of known signature genes (Figure S1A). MG ductal basal cells (cluster 3) were marked by expression of *Col17a1* and *Ki67* (Figure S1A, E, F);

ductal suprabasal cells (cluster 8) by high levels of *Krt17* and *Egr2* (Figure S1A, F); orifice cells (cluster 11) by *Krt10*, *Flg* and *Lor* (Figure S1A, G, H); acinar basal cells (cluster 16) by expression of *Pparg*, *Ki67* and *Slc1a3* (Figure 1A, I, J); ductular cells (cluster 17) by moderate expression of *Krt17* and *Lrig1*, and low levels of *Slc1a3* and *Pparg* (Figure S1A, J); differentiating meibocytes (cluster 24) by expression of *Fasn* and high levels of *Pparg* (Figure 1A, I, K); and differentiated meibocytes (cluster 18) by expression of *Scd4* and lack of *Fasn* expression (Figure 1A, K, L). Non-MG populations included conjunctival cells (clusters 0-2, 4-7, 9, 10, 12, 13, 25, 28, 30, 31), HF epithelial cells (clusters 14, 19, 26), HF dermal papilla cells (cluster 32), eyelid dermal cells (cluster 15 and 23), immune cells (cluster 20), endothelial cells (clusters 21 and 29), melanocytes (cluster 33), and muscle cells (clusters 22 and 27).

To verify the accuracy of these annotations, we conducted spatial transcriptomic analysis and integrated the outcomes of the two assays. These analyses showed that annotation of MG cell populations based on snRNA-seq data was congruent with their anatomical positions within the tarsal plate (Figure S1M).

Comparison of these data with published single-cell analysis of the HF-associated SG[16] revealed many commonalities, including expression of low levels of *Pparg* in acinar basal cells. A key difference was that MG acinar basal cells and ductular cells expressed genes associated with neural guidance, including *Slit3*, *Robo2*, *Sema3a* and *Epha7*, that were not notably expressed in HF-associated SG basal cells[16]. In line with this, MGs, but not HF-associated SGs, are directly innervated[24-27].

We used Velocity and pseudotime analyses to analyze the snRNA-seq data for the differentiation trajectories of MG cell populations. These analyses predicted that ductal basal cells give rise to ductal suprabasal cells, while acinar basal cells produce progeny that form

differentiating acinar cells, which further differentiate into differentiated acinar cells (Figure 1B, C). These predictions are in line with those for HF-associated SGs[16]. Interestingly, ductular cells appeared to contribute to both ductal and acinar basal cell populations (Figure 1B), suggesting that the ductules contain mixtures of stem cells fated to become either duct or acinus, and/or harbor bi-potential stem cells[28].

MG acinar basal cells and ductular cells express HF and SG stem cell markers

Specific markers for MG stem cells are poorly defined. As MGs share many characteristics with HF-associated SGs we interrogated the snRNA-seq data for known SG stem cell markers and validated the results using RNAscope assays on independent biological samples of adult MG. Our analysis (Figure S2A, B) showed that expression of *Lrig1* in ductular cells and ductal suprabasal cells was similar to that of the putative MG stem cell marker *Egr2* (Figure S2C, D). We found that acinar basal cells (cluster 16) expressed the SG stem cell markers *Lgr6* (Figure S2A, B; Figure S2F, white arrow) and *Slc1a3*[29] (Figure S2A, B; Figure S1J, white arrows), and also exhibited low-level expression of *Lrig1* (Figure S2A, B; Figure S2E, white arrow) and *Axin2*[30] (Figure S2A, B; Figure S2G, white arrows), along with expression of *Gli2* (Figure S2A, B; Figure S2H, white arrow). Ductular cells (cluster 17) were also enriched for *Gli2* expression (Figure S2A, B; Figure S2H, yellow arrows) and expressed high levels of *Lrig1* (Figure S2A, B; Figure S2E, yellow arrows), together with low levels of *Lgr6*, *Axin2*, and *Slc1a3* (Figure S2A, B; yellow arrows in Figure S2F, G and Figure S1J). *Slc1a3* expression only localized to the acinus and ductule and was absent from the duct (Figure S2A, B; Figure S1J), like its expression in SGs[29]. The expression of SG stem cell markers in the acinar basal layer and ductule suggested that these markers may also label stem cells within the MG.

***Lrig1*-, *Lgr6*-, *Axin2*-, *Slc1a3*-, and *Gli2*-expressing cells contribute to MG homeostasis**

To determine whether *Lrig1*-, *Lgr6*- and *Axin2*-expressing cells self-renew and contribute to MG homeostasis, we performed lineage tracing assays using *Lrig1-Cre*^{ERT2}, *Lgr6-Cre*^{ERT2}, *Axin2-Cre*^{ERT2}, *Slc1a3-Cre*^{ERT2}, and *Gli2-Cre*^{ERT2} mice carrying a *Rosa26*^{mTmG} or *Rosa26*^{nTnG} reporter allele (Figure 1D). After 2 days of tamoxifen induction, we observed *Lrig1-Cre*^{ERT2}-labeled cells in MG ducts (Figure 1E, yellow arrows) and in acinar basal cells (Figure 1E, white arrow), in line with expression of endogenous *Lrig1*. As the complete maturation process of meibocytes from acinar basal cells in mice takes approximately 9 days[31], we analyzed the descendants of *Lrig1*-expressing cells after 120 days of tracing, which is sufficient time for labeled cells to undergo multiple rounds of cell renewal. We found that progeny of *Lrig1*-expressing cells were present in both MG ducts (Figure 1E, light blue arrows) and acini (Figure 1E, pink arrow), indicating that these cells can self-renew and give rise to differentiating progeny.

Similarly, we found that cells labelled by *Lgr6-Cre*^{ERT2} were present in both MG ducts and acini after 2 days of tracing (Figure 1F); after 90 days of tracing, GFP+ descendants of *Lgr6*-expressing cells were present in both MG ducts and acini (Figure 1F).

Axin2-Cre^{ERT2}-labeled cells were detected in MG ducts and acini at 2 days after Cre induction; after 120 days, GFP+ descendants of *Axin2*-expressing cells were observed in MG ducts and acini (Figure 1G).

Interestingly, although at 2 days after Cre induction *Gli2-Cre*^{ERT2}-labeled cells were exclusively present in ductules (Figure 1H, orange arrowhead) and acini (Figure 1H, white and pink arrows), at 90 days, GFP+ descendants of *Gli2*-expressing cells not only replenished the ductule (Figure 1H, orange arrowhead) and acinus (Figure 1H, white and pink arrowheads), but also contributed to the central duct (Figure 1H, yellow and white arrowheads).

In line with snRNA-seq data, at 2 days after Cre induction *Slc1a3*-labeled cells were only identified in the acinar basal layer (Figure 1I, white arrowhead), meibocytes (Figure 1I, yellow arrowhead) and ductules, and not in the central duct; at 90-days after Cre induction, GFP+ descendants of *Slc1a3*-expressing cells were present in the acinar basal layer (Figure 1I, white arrowhead) and in meibocytes (Figure1I, yellow arrowheads), but not in the central duct. Thus, *Slc1a3* marks acinar, but not duct, stem cells.

Taken together, these data demonstrate that *Lrig1*-, *Lgr6*-, *Axin2*-, *Slc1a3*, and *Gli2*-expressing populations contain self-renewing stem cells that persist through multiple rounds of MG cell renewal and give rise to differentiated progeny in the duct and/or acinus to maintain MG homeostasis. Furthermore, in line with the prediction from Velocity analysis that the progeny of ductular stem cells can contribute to ducts and acini (Figure 1B), lineage tracing with *Gli2-Cre^{ERT2}* revealed the presence of descendants of *Gli2*-expressing ductular cells in the central duct.

Lrig1+ stem cells located in the MG ductule migrate toward the acinus

A previous study identified label-retaining cells in ductules, suggesting that ductules may contain stem cells that can replenish the acinus[12]. This hypothesis was supported by Velocity analysis of our snRNA-seq data (Figure 1B). To test this further, we investigated the behavior of *Lrig1*+ cells in ductules by combining lineage tracing in *Lrig1-Cre^{ERT2} Rosa26^{nTnG}* mice, and ex vivo live imaging. After 40 days of lineage tracing, which is sufficient for the MG to undergo several turnover cycles, we identified GFP+ cell clones in the MG acinus (Figure S3A, B, yellow arrows), ductule (Figure S3A, B, white arrows), and duct (Figure S3A, B, blue arrows). Tarsal plate explants from these mice were cultured ex vivo for 60 minutes, during which period explants remained proliferative and secreted meibum droplets (Figures S4A-C, Video S1). Time-lapse imaging of tarsal plate explants from lineage-traced *Lrig1-Cre^{ERT2} Rosa26^{nTnG}* mice

over 15 hours of culture identified GFP+ cells or their daughter cells from division within the ductules that moved toward the acinus and settled in the acinar basal layer (Video S2, arrowheads). Thus, *Lrig1*+ cells in the ductule can contribute to the acinar basal layer.

Hh signaling maintains MG homeostasis

Given our finding that MG stem cells express similar markers to SG stem cells, we hypothesized that MG and SG stem cell activity are regulated by similar mechanisms. Among several signaling pathways important for SG development and homeostasis[32,33], Hedgehog (Hh) signaling plays a critical role[20]. Interrogation of the snRNA-seq dataset (Figure S5A) and validation using RNAscope (Figure S5B-E) showed that multiple Hh pathway components[34] are expressed in the MG. *Shh* is expressed in a sub-population of acinar basal cells (Figure S5B, green arrows); *Ptch1* localizes to acinar basal cells (Figure S5C, green arrows), differentiating meibocytes (Figure S5C, white arrow), and ductular cells (Figure S5C, yellow arrow); *Smo* is expressed in acinar basal cells (Figure S5D, green arrow), ductular cells (Figure S5D, yellow arrow), and ductal cells (Figure S5D, pink arrow); and *Gli1* is expressed in acinar basal cells (Figure S5E, green arrows), differentiating meibocytes (Figure S5E, white arrow), and ductular cells (Figure S5E, yellow arrow). Additionally, we noted expression of *Ptch1*, *Smo* and *Gli1* in the surrounding stroma (Figure S5C-E, light blue arrows).

To determine whether epithelial Hh signaling is functionally required for adult MG homeostasis, we inducibly deleted the Hh co-receptor *Smo* in adult MG epithelium by treating *Krt14-Cre^{ERT2} Smo$^{fl/fl}$ Rosa26^{mTmG}* mice and *Krt14-Cre^{ERT2} Rosa26^{mTmG}* littermate controls with tamoxifen for 5 days starting at 8 weeks of age. This resulted in reduced size of acini in *Smo*-deleted MGs analyzed at 18 or 29 weeks post-tamoxifen treatment (Figure 2A-C). Differentiation of MG acini was not obviously affected (Figure 2D-G), but *Smo*-deleted MGs exhibited significantly

decreased proliferation of acinar basal cells compared with controls (Figure 2H, I, J). Thus, Hh signaling maintains MG acini by promoting the proliferation of acinar basal cells.

Forced expression of GLI2ΔN in the MG epithelium causes expansion of acinar basal cells

To ask whether Hh signaling is sufficient to promote MG basal cell proliferation, we generated *K5-rtTA tetO-GLI2ΔN* (*GLI2ΔN*^{K5rtTA}) transgenic mice that expressed an activated form of GLI2 (GLI2ΔN) in basal epithelial cells, including those in the MG, in a doxycycline-dependent manner[35,36]. GLI2ΔN+ acinar basal cells emerged within 2 days of initiating doxycycline treatment (Figure 2K, L, Q, R), and began to expand, starting to replace differentiating PLIN2+ meibocytes by 4 days after induction (Figure 2M, N, S, T). After 7 days, most meibocytes had been replaced by GLI2ΔN+ cells (Figure 2O, P, U, V) that showed statistically significantly increased proliferation compared to control acinar basal cells (Figure 2W-Y). Thus, hyper-activation of Hh signaling caused expansion of acinar basal cells by promoting their proliferation.

GLI2ΔN promoted proliferation of *Lrig1*- and *Lgr6*-expressing cells at the expense of differentiation

To delineate the mechanisms responsible for GLI2ΔN-mediated acinar basal cell expansion, we performed bulk RNA-seq on MGs laser-captured from control and *GLI2ΔN*^{K5rtTA} mice after 4 days of doxycycline treatment (Figure 3A). Gene ontology (GO) enrichment analysis showed that the most significantly upregulated pathways were those involved in regulation of cell proliferation, including proliferation regulators such as *Ki67* and *Ccnd1* (Figure 3B, C), in line with IF results (Figure 2W-Y). Expression of Hh target genes *Gli1*, *Ptch1*, and *Hhip* was also significantly elevated in GLI2ΔN-expressing MGs compared to controls (Figure 3C). The most significantly downregulated genes were those associated with control of lipid metabolism

(Figure 3B) such as *Pparg*, and meibocyte differentiation including *Scd3*, *Scd4,* and *Plin2* (Figure 3C). RNAscope and IF analyses confirmed increased expression of *Gli1* and *Ccnd1* and reduced levels of PPARγ and PLIN2 expression in GLI2ΔN-expressing MGs compared to controls (Figure 3D-I). Notably, cell populations expressing MG stem cell markers *Lrig1* and *Lgr6* were expanded upon GLI2ΔN expression in MGs (Figure 3C, J-M). Collectively, these data suggest that forced GLI2ΔN expression in MG epithelium promotes proliferation, expands the number of cells expressing *Lrig1* and *Lgr6*, and, either directly or indirectly, suppresses meibocyte differentiation.

Lrig1-, Lrg6- and *Axin2*-expressing MG stem cells contribute to MG overgrowth driven by GLI2ΔN

To test whether *Lrig1*-, *Lgr6*- and *Axin2*-expressing MG stem cells contribute to basal cell expansion caused by forced GLI2ΔN expression, we performed lineage tracing in *Lrig1-Cre*^{ERT2} *Rosa26*^{mTmG}, *Lgr6-Cre*^{ERT2} *Rosa26*^{mTmG}, and *Axin2-Cre*^{ERT2} *Rosa26*^{mTmG} mice carrying *Gli2ΔN*^{K5rtTA}. Adult mice were treated with tamoxifen to induce Cre activity; after 30 days, mice were placed on doxycycline water to induce GLI2ΔN expression in MG stem cells. Two days after initiating doxycycline treatment, GFP+/GLI2ΔN+ cells were present in the acinar basal layer in each of these lines (Figure 3N, P, R, yellow arrows). After 10 days of doxycycline treatment, we observed expansion of GFP+/GLI2ΔN+ clones in all three lines (Figure 3O, Q, S, white arrows). These observations indicate that GLI2ΔN-expressing MG stem cells contribute to MG basal expansion.

Human Meibomian gland carcinoma samples express GLI2 and exhibit expansion of *LRIG1* and *LGR6*-expressing undifferentiated cells

Abnormal stem cell activity is frequently observed in cancers[37,38], but the role of stem cells in human Meibomian gland carcinoma (MGC) is unknown. To determine whether expanded GLI2

and stem cell marker expression are features of human MGC, we analyzed 7 control MG samples and 10 MGC samples. We found that in all control MGs examined, GLI2 was predominantly expressed in acinar basal cells (Figure 4A, yellow arrows) and differentiating meibocytes (Figure 4A, white arrows) but was absent in fully differentiated meibocytes (Figure 4A, light blue arrows). By contrast, GLI2 was broadly expressed in all 10 MGC samples (Figure 4B). *GLI1* was weakly expressed in acinar basal cells of control MGs (Figure 4C, yellow arrows), but was readily detected in 7 of 10 MGC samples (Figure 4D). *LRIG1* was predominantly expressed in the acinar basal layer of control MGs (Figure 4E, yellow arrows), but was broadly and strongly expressed in all 10 MGC samples (Figure 4F). Similarly, *LGR6* expression was detected in acinar basal cells of control MGs (Figure 4G, yellow arrow), but was broadly expressed in MGC samples (9/10) (Figure 4H). In control MGs, proliferation was restricted to the basal layer of the acinus (Figure 4I, white arrows), which lacked expression of differentiation marker PLIN2 (Figure 4K, white arrows). However, in MGC samples, proliferative cells were widely present (Figure 4J, yellow arrows) and PLIN2 expression was undetectable in most tumor cells (Figure 4L, yellow arrows). These data indicate that human MGC is characterized by expansion of poorly differentiated and proliferative tumor cells that express MG stem cell markers.

Aged MG display fewer cells expressing Hh pathway genes

The mechanisms underlying MG dropout in aging remain poorly understood. As previously reported[9,39], we found that in aged (21-month) versus young (8-week) MGs, intracellular distribution of PPARγ was altered, being relatively reduced in the cytoplasm and enriched in the nucleus in aged samples (Figure S6A, B), while the percentage of KRT5+ acinar basal cells that were positive for the proliferation marker Ki-67 was significantly decreased in aged compared with young MGs (Figure S6C, D, E).

As our data revealed a key role for Hh signaling in acinar basal cell proliferation, we asked whether expression of Hh pathway genes was altered in aging. Analysis of snRNA-seq data from young and aged MGs using CellChat, which assesses intercellular communication based on patterns of ligand and cognate receptor expression[40], predicted that in young mice, IHH ligands secreted from MG ductal cells and differentiating Meibocytes are received by ductular cells, acinar basal cells, and dermal cells (Figure S6F, G). However, in aged mice, the levels of Hh pathway gene expression were decreased to the point that significant Hh-mediated interactions could not be identified (Figure S6H, I). Violin plots derived from snRNA-seq data showed that the percentages of ductular cells expressing *Gli2* and acinar basal cells expressing *Ptch1* were reduced in aged versus young MGs (Figure 5A). Validation by RNAscope revealed that there were fewer cells expressing *Ptch1* in the acinar basal layer, differentiating meibocyte population, and stroma in aged MG (Figure 5C) compared with MG at 8 weeks (Figure 5B). Similarly, there were fewer cells expressing *Gli2* in aged compared with young MG, especially in the ductules (Figure 5D, E, white arrows).

Association of GLI2 with acetylated lysine is increased in aged MGs

Despite reduced Hh pathway activity, expression of Hh ligands was maintained in aged MG (Figure 5F, G), suggesting that mechanisms other than decreased ligand expression downregulate Hh signaling in aged MGs. Proximity ligation assays (PLA) revealed that subsets of cells in aged MG acini (Figure 5H, I, white arrows) and surrounding stroma (Figure 5H, I, blue arrows) displayed elevated association of GLI2 protein with acetylated lysine. Acetylation mitigates the transcriptional activity of GLI2[41]; thus, this mechanism could potentially account for the observed decrease in the percentages of cells expressing Hh target genes in MGs and their stromal environment.

MGs with epithelial deletion of the histone deacetylases HDAC1 and HDAC2 exhibit reduced proliferation of acinar basal cells[42]. As GLI2 can be deacetylated by HDAC1[42], we hypothesized that association of GLI2 with acetylated lysine would be increased in the absence of HDAC1/2. In line with this, *Hdac1/2*-deleted acinar basal and differentiating cells in MGs from 8-week-old *K5-rtTA tetO-Cre Hdac1*$^{fl/fl}$ *Hdac2*$^{fl/fl}$ mice that had been doxycycline-treated for 10 days, showed increased PLA signals for GLI2 and acetylated lysine (Figure 5J, K, white and yellow arrows). PLA signals in the surrounding stromal cells, where *Hdac1/2* were not deleted, were similar in mutant and control mice, providing an internal control for the PLA assay (Figure 5J, K, blue arrows). Furthermore, *Ptch1* expression was attenuated within HDAC1/2-deficient acini (Figure 5L, M, white and yellow arrows) but not in the surrounding stroma (Figure 5L, M, blue arrows). Violin plots derived from snRNA-seq data revealed similar numbers of ductular cells expressing *Hdac1* and increased numbers expressing *Hdac2* in aged versus young MGs; and decreased numbers of acinar basal cells expressing *Hdac1* and increased numbers expressing *Hdac2* in aged versus young MGs (Figure 5N). IF assays failed to detect a discernable difference in the expression of HDAC1/2 proteins between young and aged MG acini (Figure 5O, P). Thus, mechanisms that affect HDAC1/2 activity, rather than altered expression levels of these proteins, may account for increased association of GLI2 with acetylated lysine in aged MGs.

Taken together these observations suggest that the decreased percentages of cells exhibiting Hh activity in aged MG and the surrounding stroma may result in part from increased levels of GLI2 acetylation that mitigate its transcriptional activity in subsets of acinar and stromal cells.

Decreased HBEGF signaling is associated with MG aging

Abrogation of epithelial Hh signaling in adult life did not result in complete loss of MGs, suggesting important contributions of additional signaling pathways to MG maintenance and the loss of these functions in aging. CellChat analysis of snRNA-seq data from young and aged

MGs predicted that the EGF pathway contributes to intercellular communication among MG subpopulations and between MG epithelial cells and the surrounding dermal niche and is attenuated in aged mice (Figure 6A, B). CellChat analysis specifically predicted that HBEGF-EGFR-mediated crosstalk between dermal cells and ductular and acinar basal cells is abolished in aged MG (Figure 6C, green pathways). Analysis of snRNA-seq data showed that the relative percentages of cells expressing *Hbegf* were reduced in aged versus young differentiating meibocyte, acinar basal, and dermal fibroblast populations (Figure 6D). These data were validated via RNAscope analysis of independent samples which revealed fewer *Hbegf*-expressing cells and decreased *Hbegf* expression levels per cell in the aged versus young acinar basal layer (Figure 6E, yellow arrows) and stroma (Figure 6E, white arrows). In line with this, phosphorylation of ERK1/2 (p-ERK1/2), which can be stimulated by EGFR activation[43], was decreased in aged MG (Figure 6F). Taken together with known pro-proliferative functions for EGF signaling in cultured human or rabbit MG epithelial cells in vitro[44,45], and in mouse eyelid and MG morphogenesis in vivo[46], these results suggest that the HBEGF-EGFR axis is important for MG homeostasis and that its decreased activity contributes to reduced proliferation of acinar basal cells in aged MG. Other pathways predicted to be dysregulated in aging included FGF signaling (Figure 6A, B), consistent with the role of FGF signaling in sebaceous gland regeneration[16], and results from bulk RNA-seq of young and old tarsal plates[47].

Aging disrupts the MG microenvironment

To delineate additional mechanisms that may contribute to the aging of MG, we performed GO analysis of differentially expressed genes in snRNA-seq data from young and aged MGs. Unexpectedly, the results showed statistically significant aging-related decreases in the expression levels of neural guidance genes such as *Slit3*, *Robo2*, *Sema3a* and *Epha7* in the MG acinar basal layer and surrounding dermal cells (Figure 7A, B, E, F). These data were validated by RNAscope (Figure 7C, D). These findings, together with the known impact of

sensory nerves on MG epithelial cells[48], and decreased peripheral innervation of the lacrimal gland in aged mice[49,50], suggested that altered peripheral nerve function could contribute to MG defects in aging. Consistent with this, IF for the pan-neural marker PGP9.5[25] revealed that the density of nerves near MG acinar basal cells was compromised in aged compared to young mice (Figure 7G-I).

In addition to the neuron-regulatory genes, downregulated DEGs in aged eyelid dermal fibroblasts included those responsible for collagen synthesis and extracellular matrix assembly, such as *Col1a1*, *Col1a2* and *Col3a1* (Figure 7J-M), in line with previous data indicating disrupted collagen synthesis in aged dermal fibroblasts[51].

By contrast, upregulated DEGs in aged MG acinar basal cells and ductular cells were associated with oxidative and other forms of stress (Figure S7A-D), which contribute to aging in other contexts[52,53], while upregulated DEGs in aged MG dermal cells were associated with inflammation, consistent with immune cell infiltration in aged MGs[6] (Figure S7E-H).

Taken together, our analyses of aged versus young MGs revealed that MG aging is associated with multiple potential mechanisms, including decreased Hh and EGF signaling, altered function of peripheral neurons, a disrupted dermal microenvironment, and inflammation.

Discussion

Little is known about the molecular identities, locations, and behavior of MG stem cells, the signaling pathways that control their homeostasis, and the nature of their tissue niche. Improved understanding of these properties will be important in identifying effective treatments for

evaporative dry eye disease, which are currently lacking. To begin to address these questions we used snRNA-seq and lineage tracing approaches to identify MG stem cells, showed that Hh signaling plays a key role in MG stem cell proliferation, and uncovered decreased Hh and EGF signaling in aged compared with young MGs.

Prior data showed that distinct basal cell populations replenish the central MG ducts and the acini, but specific markers for these stem cell sub-populations had not been identified. We found that basal stem cells marked by *Slc1a3* exclusively contribute to the acinus; by contrast, lineage tracing analyses revealed that both duct and acinus were replenished by stem cells that expressed *Lrig1*, *Lgr6, Axin2* or *Gli2*.

MG ductules, which connect the central duct and the acini, contain label-retaining cells and have been suggested to contribute to MG homeostasis[12]. However, experimental evidence for this concept has been lacking. Our snRNA-seq analysis revealed that ductules express genes that are characteristic of both the MG duct (*Krt17* and *Egr2*) and the acinus (*Pparg* and *Slc1a3*). Velocity analysis of the snRNA-seq data predicted that ductular cells contribute to both the central duct and the acinus. In line with this, we found that ductular cells express *Slc1a3* as well as *Lrig1*, *Lgr6*, *Axin2*, and *Gli2*. Lineage tracing combined with live imaging of MG explants showed that LRIG1+ cells in the ductule can migrate towards the acinus. Furthermore, *Gli2* expression is absent in the central duct, but ductular cells lineage-traced for *Gli2* populate the central duct. Taken together, these results indicate that the ductule harbors stem cells for both duct and acinus.

Our snRNA-seq data and analyses of mice lacking the Hh receptor Smo revealed that Hh signaling plays a key role in promoting proliferation of MG stem cells. Consistent with this, forced expression of activated GLI2 in MG epithelial cells resulted in expansion of stem cell

populations. We found that, like in mouse GLI2ΔN-expressing MGs, human GLI2+ MGC cells are proliferative and poorly differentiated, exhibiting broad and increased expression of the stem cell markers *LRIG1* and *LGR6*, suggesting that they arise from uncontrolled stem cell expansion. To date, genetic mutations of Hh components have not been identified in MGC. This may partially be attributed to the low occurrence of this disease. Alternatively, genes controlling posttranslational modification of GLI2, such as those regulating its acetylation[41,54] and ubiquitination[55], may be mutated or disrupted in MGC. Further investigation is required to test these potential mechanisms.

The observed decline in Hh pathway activity in aged MG could contribute to aging-associated reduced proliferation and MG dropout. Expression levels of Hh ligands were similar in young and aged MGs; however, association of GLI2 with acetylated lysine, which dampens its transcriptional activity, was increased in aged compared with young MG epithelial and surrounding stromal cells. GLI2 is deacetylated by the histone deacetylases HDAC1/2, and we found that association of GLI2 with acetylated lysine was increased in HDAC1/2-deficient MGs. Consistent with this, we previously showed that depletion of epithelial HDAC1/2 causes decreased MG basal cell proliferation[42]. Taken together, these data support a model in which decreased Hh signaling in aging results in part from altered HDAC1/2 activity that impacts GLI2.

Deletion of epithelial *Smo* did not result in complete loss of MGs, indicating the existence of additional critical pathways. Analysis of snRNA-seq data using CellChat predicted the existence of HBEGF signaling between dermal fibroblasts and both acinar and ductular basal cells that was strongly decreased in aging. This prediction was validated by analysis of *Hbegf* and p-ERK1/2 expression in independent samples of young and aged MGs and is consistent with in vitro experiments showing that EGFR activation is sufficient to stimulate the proliferation of MG epithelial cells[44,45]. Further investigations will be needed to determine the precise role of

HBEGF-EGFR signaling in MG homeostasis and the mechanisms controlling its activity during aging.

The MG is highly innervated[25-27], neurotransmitters can stimulate proliferation of MG epithelial cells in vitro[48], and impaired innervation and/or neurotransmitter secretion have been observed during aging in other glands such as the exorbital lacrimal gland[56] and sweat gland[57]. However, the in vivo functions of MG innervation and how these might be altered in aging have not been examined. Our studies revealed that impaired innervation is a previously uncharacterized feature of aged MG and may result from decreased expression of axon guidance factors in aged MG epithelial cells and surrounding dermis[58,59].

In summary, our data identify markers for the distinct stem cell populations that maintain MG ducts and acini and reveal that MG ductules harbor stem cells for both the duct and the acinus. We uncovered Hh signaling as a key pathway regulating MG stem cell proliferation and showed that its activity is enhanced in human MGC and decreased in aging. We further found that decreased HBEGF signaling, reduced peripheral innervation, and an altered dermal microenvironment accompany MG aging and may contribute to reduced epithelial proliferation and MG dropout. These observations provide a new understanding of the mechanisms of MG homeostasis, aging, and tumorigenesis, and suggest Hh signaling as a therapeutic target in MGC and in MG aging. Transient, localized and tightly controlled Hh and EGFR pathway activation could provide therapeutic benefit for patients with evaporative dry eye disease by stimulating stem cell activity, whereas inhibition of the Hh pathway, for instance with SMO inhibitors[60], may be useful in treatment of MGC.

Limitations of Study

snRNA-seq, spatial transcriptomics, and aging-related experiments were carried out in male mice. While most validation experiments were performed on both male and female samples, lack of inclusion of female samples in the snRNA-seq dataset and in aging-related experiments could mean that sex-specific differences in MG biology and aging were missed in the current study.

Acknowledgments

We thank Dr. Rachel Brody and the Institutional Biorepository & Pathology Core, Icahn School of Medicine at Mount Sinai, New York, USA for de-identified human eyelid tissue; Dr. Robert Sebra and the Genomics Core Facility, Icahn School of Medicine at Mount Sinai, New York, USA for snRNA sequencing and spatial transcriptomics; Dr. Steven Prouty for advice on laser capture; Drs. Elaine Fuchs and Michael Rendl for *KRT14:H2BGFP* mice; Dr. Adam Glick for *K5-rtTA* mice; and Dr. Eric N. Olson for *Hdac1*$^{fl/fl}$ and *Hdac2*$^{fl/fl}$ mice. This work was supported by NIH grants R01AR081322 (SEM), R37AR047709 (SEM), R01EY035337 (CI), R01EY036135 (CI), and a pilot grant from the NIAMS/NIH-supported Skin Biology and Diseases Resource-based Center (SBDRC) P30AR079200 (XZ).

Author contributions

Conceptualization: XZ, MX, SEM; Formal Analysis: XZ, MX; Funding Acquisition: XZ, SEM; Investigation: XZ, MX, CP, YL, AF; Methodology: XZ, MX; Project Administration: SEM; Resources: XZ, RB, VL, JS, CI, TP, EEM, AAD, JMC, SEM; Supervision: SEM; Validation: XZ, MX; Visualization: XZ, MX; Writing - Original Draft Preparation: XZ; Writing - Review and Editing: XZ, MX, CI, SEM.

Declaration of interests

The authors declare no competing interests.

Data availability statement

The authors declare that the main data supporting the findings of this study are available within the article and its Supplemental Information files. This study did not generate unique new reagents. snRNA-seq, spatial transcriptomics, and bulk RNA-seq datasets will be accessible through the GEO website on publication. Further information and requests for resources and reagents should be directed to and will be fulfilled by the lead contact, Sarah E. Millar (sarah.millar@mssm.edu).

Supplemental information

Document S1. Figures S1-S7 and legends for Videos S1 and S2.

Video S1. MGs in tarsal plate explants undergo proliferation and secrete lipid droplets during short-term culture. Related to Figure 1.

Video S2. Lrig1+ MG ductule stem cell progeny can migrate toward acinus and locate in the acinus basal layer. Related to Figure 1.

Figure Legends

Figure 1. Identification of distinct MG stem cell populations. (A) UMAP plot of snRNA-seq data from pooled tarsal plate samples from four 8-week-old and four 21-month-old male mice, respectively, with two replicates for each age. (B, C) RNA Velocity (B) and pseudotime analyses (C) predictions of the differentiation trajectories of MG cellular subpopulations. RNA Velocity (B) predicts that ductular cells can differentiate towards either duct or acinus. (D) Scheme for lineage tracing. (E) *Lrig1*+ cells in MG ductal basal layer (yellow arrows) and acinar basal layer (white arrow) self-renew and generate progeny that contribute to MG duct (light blue arrows) and acinus (pink arrow). (F) *Lgr6*+ cells in MG duct (yellow arrows) and acinar basal layer (white arrow) self-renew and contribute to MG duct (light blue arrow) and acinus (pink arrow). (G) *Axin2*+ cells in the MG duct (yellow arrows) and acinar basal layer (white arrow) self-renew and replenish MG duct (light blue arrow) and acinus (pink arrow). (H) At 2 days, *Gli2* marks acinar basal cells (white arrowheads), ductules (orange arrowhead), and meibocytes (white arrowheads); at 90 days, lineage-traced cells are present in MG duct (yellow and green blue arrowheads), ductule (orange arrowhead) and acinus (white and pink arrowheads). (I) At 2 days, *Slc1a3* marks meibocytes (yellow arrowhead) and acinar basal cells (white arrowhead); at 90 days, lineage tracing labels the acinar basal layer (white arrowhead) and meibocytes (yellow arrowheads). Scale bars: (B-D), 50μm; (E, G-K), 25μm. White dashed lines in (E-I) outline MG acini and ducts. 3 mice of each genotype were analyzed in lineage tracing experiments for each line and stage. See also Figures S1-S4; Video 1; Video 2.

Figure 2. Hh signaling promotes and is required for normal levels of acinar basal cell proliferation. (A-C) Whole-mount fluorescence images of MG #6 and/or MG #7 in (A) *KRT14-Cre^{ERT2} Rosa26^{mTmG}* control mice 29 weeks after tamoxifen treatment (T29Weeks); (B) *KRT14-Cre^{ERT2} Smo$^{fl/fl}$ Rosa26^{mTmG}* mice 18 weeks after tamoxifen treatment (T18 Weeks); (C) *KRT14-*

Cre^{ERT2} *Smo*$^{fl/fl}$ *Rosa26*^{mTmG} mice at T29 Weeks. Yellow asterisks indicate hair follicles; CD, MG central duct. (D-G) IHC for PPARγ (D, E) and FASN (F, G) showing similar expression levels in control (D, F) and *Smo*-deficient (E, G) MGs at 34 weeks after tamoxifen treatment. (H, I) IHC for Ki-67 showing reduced acinar basal cell proliferation in *Smo*-deficient MGs at 34 weeks after tamoxifen treatment (I) compared with control (H, green arrowheads). (J) Quantitation of the % of Ki-67+ cells in the acinar basal layer of control and *Smo*-deficient MGs. Littermate pairs were compared. Statistical significance was calculated using a paired two-tailed Student's *t*-test. N=4 control and N=4 *Smo*-deficient mice were analyzed at each stage. At least 70 acinar basal cells were analyzed per mouse. (K-P) Progressive expansion of acinar basal cell clusters (black arrows) in GLI2ΔN-expessing MG after 2 (K, L), 4 (M, N) and 7 (O, P) days of doxycycline treatment. Meibocytes were reduced by 7 days (P, green arrows). (Q-V) Progressive expansion of GLI2ΔN+/KRT5+ cells (yellow arrows) and reduction of PLIN2+ meibocytes (white arrows) in *Gli2ΔN*^{K5rtTA} MG acini after 2 (Q, R), 4 (S, T) and 7 (U, V) days of doxycycline treatment. (W, X) Hyperproliferation of GLI2ΔN+ cells in *Gli2ΔN*$^{K5\text{-}rtTA}$ MG acini (yellow arrow). (Y) Quantification of acinar basal cell proliferation. Samples from n=5 control mice lacking *K5-rtTA* or *tetO-GLI2ΔN* and samples from n=5 *Gli2ΔN*$^{K5\text{-}rtTA}$ mice were analyzed. At least 100 acinar cells were analyzed from each animal. Statistical significance was calculated with unpaired two-tailed Student's t-test. Data are presented as mean +/- SEM. Scale bars: 50 μm. See also Figure S5.

Figure 3. Forced GLI2ΔN expression expands MG stem cell populations and impedes meibocyte differentiation. (A) Scheme for bulk RNA-seq of laser-captured MG samples. (B) GO enrichment analysis of bulk RNA-seq data from *GLI2ΔN*^{K5rtTA} and littermate control MGs 4 days after induction showing the top 10 enriched pathways. (C) Volcano plot showing genes upregulated or downregulated at 4 days. N=3 *GLI2ΔN*^{K5rtTA} samples and n=3 littermate controls lacking *K5-rtTA* or *tetO-GLI2ΔN*; differentially expressed genes were defined as padj<0.001 and

$Log_2FC<-0.5$ or $Log_2FC>0.5$. (D-G) RNAscope showing upregulation of *Gli1* and *Ccnd1* in *GLI2ΔN*^{K5rtTA} MGs. (H-I) IF data showing decreased PPARγ and PLIN2 expression in *GLI2ΔN*^{K5rtTA} acini. (J-M) RNAscope showing expanded *Lrig1* and *Lgr6* expression in *GLI2ΔN*^{K5rtTA} MGs. Independent samples from 3 *Gli2ΔN*$^{K5\text{-}rtTA}$ mice and 3 littermate controls of genotypes *tetO-GLI2ΔN* or *K5-rtTA* were used for RNAscope and IF; all mice were doxycycline-treated for 4 days. (N-S) *GLI2ΔN*$^{K5\text{-}rtTA}$ *Rosa26*^{mTmG} mice carrying inducible Cre alleles driven by *Lrig1* (N, O), *Lgr6* (P, Q) or *Axin2* (R, S) promoters were tamoxifen induced at P42 to induce Cre activity and placed on oral doxycycline at P72 to induce GLI2ΔN expression. mGFP expression (red signal) and GLI2 expression (green signal) were analyzed by IF at P74 (N, P, R) or P82 (O, Q, S). GLI2ΔN-expressing cells in the acinar basal layer positive for *Lrig1* (N), *Lgr6* (P) or *Axin2* (R) (yellow arrows) give rise to clones that contribute to MG overgrowth (O, Q, S, white arrows). N=3 samples were analyzed per line per time point. Scale bars: (D-M), 50 μm; (N-S), 25 μm.

Figure 4. GLI2-, *LRIG1*- and *LGR6*-expressing undifferentiated cells are expanded in human MGC. (A, B) In normal human MG GLI2 protein localizes to acinar basal cells (A, yellow arrows) and differentiating meibocytes (A, white arrows) but is absent from fully differentiated meibocytes (A, light blue arrows); in MGC samples GLI2 is broadly expressed (B). (C, D) In normal human MG, *GLI1* mRNA is weakly expressed in some acinar basal cells (C, yellow arrows); *GLI1*+ cells are widely present in MGCs (D). (E-H) *LRIG1*+ and *LGR6*+ cells are primarily present in the acinar basal layer of normal human MGs (E, G, yellow arrows); MGC displays expansion of *LRIG1*+ and *LGR6*+ cells (F, H). (I, J) Ki-67+ cells localize to the normal human acinar basal layer (I, white arrows) and are expanded in MGC (J, yellow arrows). (K, L) PLIN2-/KRT14+ cells are restricted to the acinar basal layer in normal human MG (K, white arrows) but are present throughout MGC tissue (L, yellow arrows). 7 normal human MG and 10 human MGC samples were analyzed; representative data are shown. Scale bars: 50 μm.

Figure 5. Aged MGs exhibit fewer cells with Hh activity and elevated association of GLI2 with acetyl-lysine. (A) Violin plots derived from snRNA-seq data show relatively reduced percentages of cells expressing *Gli2* and *Ptch1* in the ductule and acinar basal layer, respectively, in aged compared to young MGs. (B, C) *Ptch1* is expressed in acinar basal cells (B, white arrow), some meibocytes (B, yellow arrow), and surrounding stromal cells (B, blue arrow) at 8 weeks; fewer *Ptch1*-expressing cells are present in aged MG (C). (D, E) Fewer *Gli2*-expressing cells are present in aged MG particularly in the ductule (D, E, white arrows). (F, G) RNAscope using a pan-*Hh* probe reveals similar expression of mRNA for Hh ligands in the acini of young (F) and aged (G) MGs. (H, I) PLA for GLI2 and acetyl-lysine shows that close association (<40nm) of GLI2 with acetyl-lysine is elevated in subsets of cells within aged (I) compared with young (H) MG acini (I, white arrows) and stroma (I, blue arrows). (J, K) Association of GLI2 and acetyl-lysine is elevated in the acinar basal layer (K, white arrows) and meibocytes (K, yellow arrows) but not stromal cells (J, K, blue arrows) in *K5-rtTA tetO-Cre* *Hdac1*$^{fl/fl}$ *Hdac2*$^{fl/fl}$ (*Hdac1/2*^{DcKO}) mice doxycycline induced from P48 and analyzed at P58 compared to control mice of genotype *Hdac1*$^{fl/fl}$ *Hdac2*$^{fl/fl}$ and lacking *K5-rtTA* or *tetO-Cre.* (J). (L, M) *Ptch1* expression in control acinar basal cells (L, white arrows) and differentiating acinar cells (L, yellow arrow) is reduced in HDAC1/2-deficient MG acini (M); stromal *Ptch1* expression is similar in mutants and controls (L, M, blue arrows). (N) Violin plots of snRNA-seq data indicate that there is a relatively lower percentage of *Hdac1*-expressing acinar basal cells (cluster #16) but a higher percentage of *Hdac2*-expressing acinar basal cells and ductular cells (cluster #17) in aged compared to young MG. (O, P) IF for HDAC1/2 shows similar expression in young (O) and aged (P) MGs. White dashed lines in (B-M; O, P) outline MG acini and/or ducts. 3 mice of each age and genotype were used for RNAscope and PLA. Scale bars: 25 μm. See also Figure S6.

Figure 6. HBEGF signaling is disrupted in aged MGs. (A, B) CellChat analysis predicts decreased EGF signaling in aged MGs. (C) CellChat analysis predicts HBEGF signaling between dermal cells and MG ductular cells (green) at 8-weeks and its absence at 21-months. (D) Violin plots of snRNA-seq data show decreased percentages of *Hbegf*-expressing cells in the indicated cell populations in aged MG. (E) RNAscope shows reduced *Hbegf* expression levels per cell and fewer acinar basal cells (yellow arrows) and surrounding dermal cells (white arrows) expressing *Hbegf* in aged MG. (F) IHC shows that p-ERK1/2 levels are decreased but total ERK1/2 levels are similar in the acini of aged compared with young MG. White dashed lines in (E) and black dashed lines in (F) outline MG acini. Three pairs of 8-week and 21-month samples were used for RNAscope and IHC. Scale bars represent 25 μm.

Figure 7. Aged MGs exhibit reduced peripheral innervation and collagen I expression. (A) GO analysis of genes with statistically significantly reduced expression in aged compared with young acinar basal cells (cluster #16). (B) Violin plots for neuronal guidance genes in acinar basal cells. (C, D) *Slit3* mRNA expression (yellow arrows) is reduced in aged MG acinar basal cells. (E, F) GO analysis of genes with reduced expression in aged cluster #23 dermal cells (E) and violin plots for neuronal guidance genes (F). (G, H) Reduced numbers of PGP9.5 nerve fibers (red) adjacent to the KRT5+ acinar basal layer (green) in aged mice. (I) Quantification of PGP9.5+ nerve fibers within 5 μM of each KRT5+ acinar basal cell in young and aged MGs. Four pairs of 8-week-old and 21-month-old male mice were used for quantification. At least 185 acinar basal cells were analyzed from each mouse. Significance in (I) was calculated by an unpaired two-tailed Student's t-test. Data are represented as mean +/- SEM. (J, K) GO analysis of genes with reduced expression in aged cluster #15 dermal fibroblasts (J) and violin plots for type I collagen genes in dermal fibroblasts (K). (L, M) Reduced expression of *Col1a1* (red) in aged (M) versus young (L) dermis surrounding MG acini. White dashed lines in (C, D, L, M)

outline MG acini and/or ducts. 3 pairs of 8-week and 21-month samples were used for RNAscope, IF and IHC. Scale bars represent 25 μm. See also Figure S7.

STAR Methods

Mice

C57BL/6J mice (Jackson Laboratory #000664) were used for snRNA-seq, spatial transcriptomics, and aging-related experiments. All other mice were maintained on a mixed-strain background. Up to five mice were maintained per cage in a specific pathogen-free barrier facility using standard rodent laboratory chow. Mice of both sexes were analyzed in all experiments except for snRNA-seq, spatial transcriptomics, and aging-related experiments, and no significant sex-based differences were noted. The following mouse lines were utilized: *Lrig1-Cre*^{ERT2} (Jackson Laboratory, #018418), *Lgr6-Cre*^{ERT2} (Jackson Laboratory, #016934), *Axin2-Cre*^{ERT2} [30], *Slc1a3-Cre*^{ERT2} (European Mouse Mutant Archive, EM:12216), *Gli2-Cre*^{ERT2} [61], *K5-rtTA* (Jackson Laboratory, #017519), *tetO-GLI2ΔN*[35], *Rosa26*^{mTmG} (Jackson Laboratory, #007676), *Rosa26*^{nTnG} (Jackson Laboratory, #023537), *KRT14:H2BGFP*[62], *KRT14-Cre*^{ERT2} (Jackson Laboratory, #005107), *Smo*$^{fl/fl}$ (Jackson Laboratory, #004526), *Hdac1*$^{fl/fl}$ *Hdac2*$^{fl/fl}$ [63], *tetO-Cre* (Jackson Laboratory #006234). All animal experiments were carried out under approved animal protocols according to institutional guidelines established by the Icahn School of Medicine at Mount Sinai IACUC or the Johns Hopkins University IACUC.

Human MG samples

De-identified human eyelid tissues discarded from unrelated surgical procedures were paraffin-embedded and sectioned for histological analysis, RNAscope and IF.

snRNA-seq

Eight 8-week-old and eight 21-month-old male mice were euthanized, and their eyelids were cut with scissors. The dorsal portion of the eyelids and the surrounding tissues near the tarsal plates were removed using a scalpel. The remaining tarsal plates containing MGs were digested

with 0.2% collagenase A in PBS for 1 hour at 37 °C. The tarsal plates were then rinsed twice with PBS and tissues surrounding the MGs were removed with fine-tip forceps. Tissues from four littermate mice were pooled together in PBS for each replicate. The MG tissue-containing solutions were then transferred into 1.5mL centrifuge tubes using Pasteur pipettes. The tissue solution was centrifuged at 300g/min for 5 minutes, the supernatant was carefully removed, and the tissue pellet was rinsed once with PBS. Isolation of nuclei was performed using the protocol (CG000375 Rev B) from 10X Genomics. RNA-seq libraries were prepared based on the 10X Genomics protocol (CG000315 Rev E) using 10000 nuclei per replicate. Single-cell separation was performed using the Chromium Next GEM Chip G Single Cell Kit. The RNA-seq libraries were sequenced in paired-end mode on an Illumina Novaseq platform with the Novaseq S4 flowcell.

Alignment of 10X Genomics data

Cell Ranger Single-Cell Software Suite (v7.0.1, 10x Genomics) was used to align and quantify sequencing data against the mm10 mouse reference genome (refdata-gex-mm10-2020-A).

Analysis of snRNA-seq data

Cell clustering and differential gene expression were analyzed using Seurat[64] (v4.3.0). For each replicate, high-quality nuclei (defined as nFeature_RNA >200 & nFeature_RNA <4500 & nCount_RNA >500 & < nCount_RNA <25000 & precent.mt < 5) were analyzed. 6676 nuclei were analyzed from 8-Week replicate 1, 10734 from 8-Week replicate 2, 8336 from 21-Month replicate 1, and 7305 from 21-Month replicate 2. The CellCycleScoring function of Seurat was applied to mitigate the effects of cell cycle heterogeneity in the datasets. The SCTransform function of Seurat was used to integrate the four datasets. In total, 34 clusters were identified with a resolution of 1. For Violin plots, the y-axis was plotted against the log normalized data from the data slot of the Seurat object. Seurat employs a global-scaling normalization method

"LogNormalize" that normalizes the feature expression (each gene) measurements for each cell by the total expression, multiplies this by a scale factor (10,000 by default), and log-transforms the result.

For RNA velocity and pseudotime analyses, bam files generated from Cell Ranger were processed using Velocyto (v0.6)'s run10x function with default parameters, resulting in loom files that contained counts of unspliced and spliced mRNAs. The loom files were merged with the h5ad files, which covered the meibomian gland clusters. Subsequently, the merged files were preprocessed with scVelo (v0.3)[65], and RNA velocity and pseudotime analyses were performed using cellDancer (v1.1)[66].

To identify DEGs, genes encoding ribosomal proteins were initially defined and removed by grepping for "^Rp(sl)" from the datasets before pseudobulk analysis using EdgeR (v3.38.4)[67]. Genes with an FDR (padj)<0.05 and $|Log_2FC|>0.5$ were considered DEGs and were subjected to gene ontology analysis with clusterProfiler (v4.4.4)[68].

The interactions among distinct MG cell types (MG ductal basal cells, ductal suprabasal cells, ductular cells, acinar basal cells, differentiating meibocytes, and differentiated meibocytes), along with surrounding dermal cells (two populations were combined in this context), were analyzed using CellChat (v1.6.1)[40]. Briefly, the normalized counts were loaded into CellChat and preprocessed with default parameters. To establish the ligand-receptor interaction database, we selected secreted signaling pathways and utilized the "projectData" function to project gene expression data onto the mouse protein-protein interaction (PPI). To visualize specific signaling pathways, we employed the setting "type=truncatedMean, trim = 0.1" to compute the communication probability (computeCommunProb) except for HH signaling (trim =0.001 was used). Core CellChat functions such as "computeCommunProbPathway", "aggregateNet",

"netAnalysis_signalingRole", and "identifyCommunicationPatterns" were applied with standard parameters for downstream analysis.

Spatial transcriptomics

The 10x Visium Spatial Gene Expression kit was employed to construct the spatial transcriptomic library, according to the manufacturer's instructions. A pair of upper and lower eyelids from an 8-week-old male mouse was dissected, sectioned at 10 μM, and mounted onto the assay slide containing four capture areas (6.5mm x 6.5mm) with spatially barcoded poly T capture probes. After permeabilization, the captured mRNAs underwent reverse transcription, followed by cleaving from the slide. cDNA amplification, fragmentation, end-repair, poly A-tailing, adapter ligation, and sample indexing were performed in accordance with the manufacturer's protocol. The resulting cDNA libraries were quantified using TapeStation (Agilent) and Qubit (Invitrogen) and then subjected to sequencing in paired-end mode on a NovaSeq instrument (Illumina) at a depth of 50,000-100,000 reads per capture spot. The sequencing data were aligned and quantified using Space Ranger Software Suite (v2.1.0, 10x Genomics) against the reference genome.

Analysis of spatial transcriptomic data

Integration of snRNA-seq data and spatial transcriptomic data was conducted through CytoSPACE (v1.0.5)[69]. Briefly, a non-normalized count-based gene expression file and a cell-type label file were generated from the snRNA-seq datasets. Additionally, a compressed spatial transcriptomes input file for CytoSPACE was created using files from Space Ranger outputs. Subsequently, all the input files were loaded into CytoSPACE with the recommended parameter settings, as detailed on the project's GitHub repository (https://github.com/digitalcytometry/cytospace).

Immunofluorescence (IF) and immunohistochemistry (IHC)

Paraffin sections were deparaffinized and rehydrated to PBS. Antigen retrieval was performed with antigen unmasking solution. Sections were washed with PBST (PBS+0.1% Tween 20) and blocked with 1% BSA for 30 minutes. Primary antibodies were applied, and the sections were incubated overnight at 4°C. For IF, sections were subjected to three washes of PBST, followed by 1-hour incubation with secondary antibodies. The sections were washed with PBST and mounted with DAPI-containing medium. For IHC, sections were washed with PBST and then incubated with 3% H_2O_2/PBST for 15 minutes, followed by two washes of PBST and 30-minute incubation with biotinylated secondary antibodies. Subsequent steps and DAB staining followed the manufacturer's instructions. The sections were dehydrated, cleared, and mounted. IF and IHC data were documented using a Leica Microsystems DM5500B microscope equipped with two cameras for fluorescent and bright field images (Leica Microsystems).

RNAscope in situ hybridization

RNAscope was performed on paraffin sections following the user's guide provided by Advanced Cell Diagnostic (ACD) using probes for *Slc1a3*, *Scd4*, *Slit3*, *Hbegf*, *Col1a1*, pan-*Hh*, *Lrig1*, *Lgr6*, *Axin2*, *Ccnd1*, *Gli1*, *Gli2*, *Ptch1*, *Smo*, *Shh*, *LRIG1*, *LGR6*, and *GLI1*.

Tamoxifen induction

200µl Tamoxifen dissolved in corn oil (10mg/ml) was injected intraperitoneally once for lineage tracing. For gene deletion, daily intraperitoneal injections were performed on five consecutive days.

Ex vivo live imaging of tarsal plate explants

Mice were euthanized, and the eyelids were dissected with scissors. Tissues surrounding the tarsal plates were removed using a surgical scalpel. The tarsal plates were placed in a 35-mm

Lumox-bottom dish, immobilized with a custom-built holder, and incubated in DMEM/F12(1:1) medium supplemented with 5% FBS for 2 hours in an environmental chamber supplied with 5% CO_2 at 37°C before imaging. A Leica SP8 laser scanning confocal microscope equipped with Power HyD detectors and an environmental chamber was used to image the cultured explants. Images were captured as z stacks at 3 µm intervals and tissues were imaged every 15 min with low laser power (<3%) with a HC PL APO CS2 10x/0.40 DRY objective lens. Stacked images were maximum projected with Leica LAS X software to generate the time-lapse video and video annotations were performed with Fiji software.

Doxycycline administration

200 µg/ml doxycycline was dissolved in 5% sucrose water and was fed to the mice and replaced every 5 days.

Bulk RNA-seq and data analysis

3 pairs of 6-week-old *Gli2ΔN*^{K5rtTA} mice and littermate controls were fed with 200µg/ml doxycycline water for 4 days. Mice were euthanized and the upper and lower eyelids were dissected, frozen sectioned at 12µm, and mounted onto polyethylene naphthalate-membrane slides (Leica Microsystems). The MGs from 25 sections from each sample were laser dissected using the gravity-assisted LMD 7000 system (Leica Microsystems) and collected by gravity assistance onto AdhensiveCap. RNA was extracted using the Qiagen All Prep DNA/RNA FFPE Kit according to the manufacturer's instructions. 50ng RNA from each laser-captured sample was used for RNA-seq library construction using the Trio RNA-Seq™ library preparation kit from Nugene. The libraries were sequenced on an Illumina HiSeq 4000 platform with the 100bp single read (SR100) method. For data analysis, Salmon (v0.9.1)[70] was used to count data against the transcriptome defined in Gencode vM18. We then annotated and summarized the transcriptome count data to the gene level with tximeta[71] and performed further annotation

with biomaRt (v0.7.0)[72]. Normalizations and statistical analyses were carried out with DESeq2 (v1.20.0)[73]. Genes with padj<0.001 and $|Log_2FC|>0.5$ were selected for GO enrichment analysis, which was carried out by clusterProfiler. The results were plotted by ggplot2 (v3.4.0) and volcano plots were generated using EnhancedVolcano (v1.14.0).

Proximity ligation assay (PLA)

PLA was carried out as previously described[30] using a DuoLink In Situ PLA kit (Sigma Aldrich). Briefly, 5 μm paraffin sections were dewaxed and rehydrated, followed by blocking with 5% donkey serum/PBS/0.8% Triton X-100 for 30 minutes and incubation with solutions containing primary antibodies overnight at 4 °C. The sections were washed with PBST and incubated in PLA probe anti-rabbit plus or anti-goat plus, and PLA probe anti-rabbit minus for 2 hours. The subsequent ligation and amplification steps followed the manufacturer's instructions. The sections were washed twice in washing buffer and once in PBS for 20 minutes each before mounting and imaging using a Leica SP8 laser scanning confocal microscope.

Statistical analyses

Statistical analysis and graphical representation were performed using Microsoft Excel 2023. Unpaired or paired two-tailed Student's *t*-test was used to calculate statistical significance between two groups of data. $P < 0.05$ was considered significant. Data were represented as mean +/- SEM.

References

1. Sun, M., Moreno, I.Y., Dang, M., and Coulson-Thomas, V.J. (2020). Meibomian Gland Dysfunction: What Have Animal Models Taught Us? Int J Mol Sci *21*. 10.3390/ijms21228822.
2. Jester, J.V., Parfitt, G.J., and Brown, D.J. (2015). Meibomian gland dysfunction: hyperkeratinization or atrophy? BMC Ophthalmol *15 Suppl 1*, 156. 10.1186/s12886-015-0132-x.
3. Obata, H. (2002). Anatomy and histopathology of human meibomian gland. Cornea *21*, S70-74. 10.1097/01.ico.0000263122.45898.09.
4. Knop, E., Knop, N., Millar, T., Obata, H., and Sullivan, D.A. (2011). The international workshop on meibomian gland dysfunction: report of the subcommittee on anatomy, physiology, and pathophysiology of the meibomian gland. Invest Ophthalmol Vis Sci *52*, 1938-1978. 10.1167/iovs.10-6997c.
5. Wolff, E., Bron, A.J., Tripathi, R.C., and Tripathi, B.J. (1997). Anatomy of the eye and orbit, 8th Edition (Chapman & Hall Medical).
6. Moreno, I., Verma, S., Gesteira, T.F., and Coulson-Thomas, V.J. (2023). Recent advances in age-related meibomian gland dysfunction (ARMGD). Ocul Surf *30*, 298-306. 10.1016/j.jtos.2023.11.003.
7. Zakrzewski, W., Dobrzynski, M., Szymonowicz, M., and Rybak, Z. (2019). Stem cells: past, present, and future. Stem Cell Res Ther *10*, 68. 10.1186/s13287-019-1165-5.
8. Clevers, H., and Watt, F.M. (2018). Defining Adult Stem Cells by Function, not by Phenotype. Annu Rev Biochem *87*, 1015-1027. 10.1146/annurev-biochem-062917-012341.
9. Nien, C.J., Massei, S., Lin, G., Nabavi, C., Tao, J., Brown, D.J., Paugh, J.R., and Jester, J.V. (2011). Effects of age and dysfunction on human meibomian glands. Arch Ophthalmol *129*, 462-469. 10.1001/archophthalmol.2011.69.
10. Hwang, H.S., Parfitt, G.J., Brown, D.J., and Jester, J.V. (2017). Meibocyte differentiation and renewal: Insights into novel mechanisms of meibomian gland dysfunction (MGD). Exp Eye Res *163*, 37-45. 10.1016/j.exer.2017.02.008.
11. Nien, C.J., Paugh, J.R., Massei, S., Wahlert, A.J., Kao, W.W., and Jester, J.V. (2009). Age-related changes in the meibomian gland. Exp Eye Res *89*, 1021-1027. 10.1016/j.exer.2009.08.013.
12. Parfitt, G.J., Lewis, P.N., Young, R.D., Richardson, A., Lyons, J.G., Di Girolamo, N., and Jester, J.V. (2016). Renewal of the Holocrine Meibomian Glands by Label-Retaining,

Unipotent Epithelial Progenitors. Stem Cell Reports *7*, 399-410. 10.1016/j.stemcr.2016.07.010.

13. Jensen, K.B., Collins, C.A., Nascimento, E., Tan, D.W., Frye, M., Itami, S., and Watt, F.M. (2009). Lrig1 expression defines a distinct multipotent stem cell population in mammalian epidermis. Cell Stem Cell *4*, 427-439. 10.1016/j.stem.2009.04.014.
14. Snippert, H.J., Haegebarth, A., Kasper, M., Jaks, V., van Es, J.H., Barker, N., van de Wetering, M., van den Born, M., Begthel, H., Vries, R.G., et al. (2010). Lgr6 marks stem cells in the hair follicle that generate all cell lineages of the skin. Science *327*, 1385-1389. 10.1126/science.1184733.
15. Fullgrabe, A., Joost, S., Are, A., Jacob, T., Sivan, U., Haegebarth, A., Linnarsson, S., Simons, B.D., Clevers, H., Toftgard, R., and Kasper, M. (2015). Dynamics of Lgr6(+) Progenitor Cells in the Hair Follicle, Sebaceous Gland, and Interfollicular Epidermis. Stem Cell Reports *5*, 843-855. 10.1016/j.stemcr.2015.09.013.
16. Veniaminova, N.A., Jia, Y.Y., Hartigan, A.M., Huyge, T.J., Tsai, S.Y., Grachtchouk, M., Nakagawa, S., Dlugosz, A.A., Atwood, S.X., and Wong, S.Y. (2023). Distinct mechanisms for sebaceous gland self-renewal and regeneration provide durability in response to injury. Cell Rep *42*, 113121. 10.1016/j.celrep.2023.113121.
17. Blank, U., Karlsson, G., and Karlsson, S. (2008). Signaling pathways governing stem-cell fate. Blood *111*, 492-503. 10.1182/blood-2007-07-075168.
18. Yang, L., Shi, P., Zhao, G., Xu, J., Peng, W., Zhang, J., Zhang, G., Wang, X., Dong, Z., Chen, F., and Cui, H. (2020). Targeting cancer stem cell pathways for cancer therapy. Signal Transduct Target Ther *5*, 8. 10.1038/s41392-020-0110-5.
19. Brownell, I., Guevara, E., Bai, C.B., Loomis, C.A., and Joyner, A.L. (2011). Nerve-derived sonic hedgehog defines a niche for hair follicle stem cells capable of becoming epidermal stem cells. Cell Stem Cell *8*, 552-565. 10.1016/j.stem.2011.02.021.
20. Allen, M., Grachtchouk, M., Sheng, H., Grachtchouk, V., Wang, A., Wei, L., Liu, J., Ramirez, A., Metzger, D., Chambon, P., et al. (2003). Hedgehog signaling regulates sebaceous gland development. Am J Pathol *163*, 2173-2178. 10.1016/S0002-9440(10)63574-2.
21. Niemann, C., Unden, A.B., Lyle, S., Zouboulis Ch, C., Toftgard, R., and Watt, F.M. (2003). Indian hedgehog and beta-catenin signaling: role in the sebaceous lineage of normal and neoplastic mammalian epidermis. Proc Natl Acad Sci U S A *100 Suppl 1*, 11873-11880. 10.1073/pnas.1834202100.

22. Kim, N., Kim, J.E., Choung, H.K., Lee, M.J., and Khwarg, S.I. (2013). Expression of Shh and Wnt signaling pathway proteins in eyelid sebaceous gland carcinoma: clinicopathologic study. Invest Ophthalmol Vis Sci *54*, 370-377. 10.1167/iovs.12-10671.
23. Qu, J.Y., Xiao, Y.T., Zhang, Y.Y., Xie, H.T., and Zhang, M.C. (2021). Hedgehog Signaling Pathway Regulates the Proliferation and Differentiation of Rat Meibomian Gland Epithelial Cells. Invest Ophthalmol Vis Sci *62*, 33. 10.1167/iovs.62.2.33.
24. Clayton, R.W., Langan, E.A., Ansell, D.M., de Vos, I., Göbel, K., Schneider, M.R., Picardo, M., Lim, X., van Steensel, M.A.M., and Paus, R. (2020). Neuroendocrinology and neurobiology of sebaceous glands. Biol Rev Camb Philos Soc *95*, 592-624. 10.1111/brv.12579.
25. Brundl, M., Garreis, F., Schicht, M., Dietrich, J., and Paulsen, F. (2021). Characterization of the innervation of the meibomian glands in humans, rats and mice. Ann Anat *233*, 151609. 10.1016/j.aanat.2020.151609.
26. Cox, S.M., and Nichols, J.J. (2014). The neurobiology of the meibomian glands. Ocul Surf *12*, 167-177. 10.1016/j.jtos.2014.01.005.
27. LeDoux, M.S., Zhou, Q., Murphy, R.B., Greene, M.L., and Ryan, P. (2001). Parasympathetic innervation of the meibomian glands in rats. Invest Ophthalmol Vis Sci *42*, 2434-2441.
28. Yang, X., Reneker, L.W., Zhong, X., Huang, A.J.W., and Jester, J.V. (2023). Meibomian gland stem/progenitor cells: The hunt for gland renewal. The Ocular Surface *29*, 497-507.
29. Reichenbach, B., Classon, J., Aida, T., Tanaka, K., Genander, M., and Goritz, C. (2018). Glutamate transporter Slc1a3 mediates inter-niche stem cell activation during skin growth. EMBO J *37*. 10.15252/embj.201798280.
30. Xu, M., Horrell, J., Snitow, M., Cui, J., Gochnauer, H., Syrett, C.M., Kallish, S., Seykora, J.T., Liu, F., Gaillard, D., et al. (2017). WNT10A mutation causes ectodermal dysplasia by impairing progenitor cell proliferation and KLF4-mediated differentiation. Nat Commun *8*, 15397. 10.1038/ncomms15397.
31. Olami, Y., Zajicek, G., Cogan, M., Gnessin, H., and Pe'er, J. (2001). Turnover and migration of meibomian gland cells in rats' eyelids. Ophthalmic Res *33*, 170-175. 10.1159/000055665.
32. Niemann, C., and Horsley, V. (2012). Development and homeostasis of the sebaceous gland. Semin Cell Dev Biol *23*, 928-936. 10.1016/j.semcdb.2012.08.010.

33. Geueke, A., and Niemann, C. (2021). Stem and progenitor cells in sebaceous gland development, homeostasis and pathologies. Exp Dermatol *30*, 588-597. 10.1111/exd.14303.
34. Katoh, Y., and Katoh, M. (2009). Hedgehog target genes: mechanisms of carcinogenesis induced by aberrant hedgehog signaling activation. Curr Mol Med *9*, 873-886. 10.2174/156652409789105570.
35. Grachtchouk, M., Pero, J., Yang, S.H., Ermilov, A.N., Michael, L.E., Wang, A., Wilbert, D., Patel, R.M., Ferris, J., Diener, J., et al. (2011). Basal cell carcinomas in mice arise from hair follicle stem cells and multiple epithelial progenitor populations. J Clin Invest *121*, 1768-1781. 10.1172/JCI46307.
36. Zhu, X., Leboeuf, M., Liu, F., Grachtchouk, M., Seykora, J.T., Morrisey, E.E., Dlugosz, A.A., and Millar, S.E. (2022). HDAC1/2 Control Proliferation and Survival in Adult Epidermis and Pre□Basal Cell Carcinoma through p16 and p53. J Invest Dermatol *142*, 77-87 e10. 10.1016/j.jid.2021.05.026.
37. Clevers, H. (2011). The cancer stem cell: premises, promises and challenges. Nat Med *17*, 313-319. 10.1038/nm.2304.
38. Clarke, M.F., and Fuller, M. (2006). Stem cells and cancer: two faces of eve. Cell *124*, 1111-1115. 10.1016/j.cell.2006.03.011.
39. Jester, J.V., and Brown, D.J. (2012). Wakayama Symposium: Peroxisome proliferator-activated receptor-gamma (PPARgamma) and meibomian gland dysfunction. Ocul Surf *10*, 224-229. 10.1016/j.jtos.2012.07.001.
40. Jin, S., Guerrero-Juarez, C.F., Zhang, L., Chang, I., Ramos, R., Kuan, C.H., Myung, P., Plikus, M.V., and Nie, Q. (2021). Inference and analysis of cell-cell communication using CellChat. Nat Commun *12*, 1088. 10.1038/s41467-021-21246-9.
41. Coni, S., Antonucci, L., D'Amico, D., Di Magno, L., Infante, P., De Smaele, E., Giannini, G., Di Marcotullio, L., Screpanti, I., Gulino, A., and Canettieri, G. (2013). Gli2 acetylation at lysine 757 regulates hedgehog-dependent transcriptional output by preventing its promoter occupancy. PLoS One *8*, e65718. 10.1371/journal.pone.0065718.
42. Zhu, X., Xu, M., and Millar, S.E. (2024). HDAC1/2 and HDAC3 play distinct roles in controlling adult Meibomian gland homeostasis. Ocul Surf *33*, 39-49. 10.1016/j.jtos.2024.04.005.
43. Wee, P., and Wang, Z. (2017). Epidermal Growth Factor Receptor Cell Proliferation Signaling Pathways. Cancers (Basel) *9*. 10.3390/cancers9050052.

44. Liu, S., Kam, W.R., Ding, J., Hatton, M.P., and Sullivan, D.A. (2013). Effect of growth factors on the proliferation and gene expression of human meibomian gland epithelial cells. Invest Ophthalmol Vis Sci *54*, 2541-2550. 10.1167/iovs.12-11221.

45. Maskin, S.L., and Tseng, S.C. (1992). Clonal growth and differentiation of rabbit meibomian gland epithelium in serum-free culture: differential modulation by EGF and FGF. Invest Ophthalmol Vis Sci *33*, 205-217.

46. Dong, F., Call, M., Xia, Y., and Kao, W.W. (2017). Role of EGF receptor signaling on morphogenesis of eyelid and meibomian glands. Exp Eye Res *163*, 58-63. 10.1016/j.exer.2017.04.006.

47. Parfitt, G.J., Brown, D.J., and Jester, J.V. (2016). Transcriptome analysis of aging mouse meibomian glands. Mol Vis *22*, 518-527.

48. Kam, W.R., and Sullivan, D.A. (2011). Neurotransmitter influence on human meibomian gland epithelial cells. Invest Ophthalmol Vis Sci *52*, 8543-8548. 10.1167/iovs.11-8113.

49. Ríos, J.D., Horikawa, Y., Chen, L.-L., Kublin, C.L., Hodges, R.R., Dartt, D.A., and Zoukhri, D. (2005). Age-dependent alterations in mouse exorbital lacrimal gland structure, innervation and secretory response. Experimental Eye Research *80*, 477-491.

50. Liu, J., Si, H., Huang, D., Lu, D., Zou, S., Qi, D., Pei, X., Huang, S., and Li, Z. (2023). Mechanisms of Extraorbital Lacrimal Gland Aging in Mice: An Integrative Analysis of the Temporal Transcriptome. Invest Ophthalmol Vis Sci *64*, 18. 10.1167/iovs.64.12.18.

51. Fisher, G.J., Varani, J., and Voorhees, J.J. (2008). Looking older: fibroblast collapse and therapeutic implications. Arch Dermatol *144*, 666-672. 10.1001/archderm.144.5.666.

52. Jomova, K., Raptova, R., Alomar, S.Y., Alwasel, S.H., Nepovimova, E., Kuca, K., and Valko, M. (2023). Reactive oxygen species, toxicity, oxidative stress, and antioxidants: chronic diseases and aging. Arch Toxicol *97*, 2499-2574. 10.1007/s00204-023-03562-9.

53. Liguori, I., Russo, G., Curcio, F., Bulli, G., Aran, L., Della-Morte, D., Gargiulo, G., Testa, G., Cacciatore, F., Bonaduce, D., and Abete, P. (2018). Oxidative stress, aging, and diseases. Clin Interv Aging *13*, 757-772. 10.2147/CIA.S158513.

54. Canettieri, G., Di Marcotullio, L., Greco, A., Coni, S., Antonucci, L., Infante, P., Pietrosanti, L., De Smaele, E., Ferretti, E., Miele, E., et al. (2010). Histone deacetylase and Cullin3-REN(KCTD11) ubiquitin ligase interplay regulates Hedgehog signalling through Gli acetylation. Nat Cell Biol *12*, 132-142. 10.1038/ncb2013.

55. Bhatia, N., Thiyagarajan, S., Elcheva, I., Saleem, M., Dlugosz, A., Mukhtar, H., and Spiegelman, V.S. (2006). Gli2 is targeted for ubiquitination and degradation by beta-TrCP ubiquitin ligase. J Biol Chem *281*, 19320-19326. 10.1074/jbc.M513203200.

56. Rios, J.D., Horikawa, Y., Chen, L.L., Kublin, C.L., Hodges, R.R., Dartt, D.A., and Zoukhri, D. (2005). Age-dependent alterations in mouse exorbital lacrimal gland structure, innervation and secretory response. Exp Eye Res *80*, 477-491. 10.1016/j.exer.2004.10.012.

57. Vilches, J.J., Ceballos, D., Verdu, E., and Navarro, X. (2002). Changes in mouse sudomotor function and sweat gland innervation with ageing. Auton Neurosci *95*, 80-87. 10.1016/s1566-0702(01)00359-9.

58. Chen, Z., Shen, G., Tan, X., Qu, L., Zhang, C., Ma, L., Luo, P., Cao, X., Yang, F., Liu, Y., et al. (2021). ID1/ID3 mediate the contribution of skin fibroblasts to local nerve regeneration through Itga6 in wound repair. Stem Cells Transl Med *10*, 1637-1649. 10.1002/sctm.21-0093.

59. Olgart, C., and Frossard, N. (2001). Human lung fibroblasts secrete nerve growth factor: effect of inflammatory cytokines and glucocorticoids. Eur Respir J *18*, 115-121. 10.1183/09031936.01.00069901.

60. Li, Q.R., Zhao, H., Zhang, X.S., Lang, H., and Yu, K. (2019). Novel-smoothened inhibitors for therapeutic targeting of naïve and drug-resistant hedgehog pathway-driven cancers. Acta Pharmacol Sin *40*, 257-267. 10.1038/s41401-018-0019-5.

61. Wang, C., de Mochel, N.S.R., Christenson, S.A., Cassandras, M., Moon, R., Brumwell, A.N., Byrnes, L.E., Li, A., Yokosaki, Y., Shan, P., et al. (2018). Expansion of hedgehog disrupts mesenchymal identity and induces emphysema phenotype. J Clin Invest *128*, 4343-4358. 10.1172/JCI99435.

62. Rendl, M., Polak, L., and Fuchs, E. (2008). BMP signaling in dermal papilla cells is required for their hair follicle-inductive properties. Genes Dev *22*, 543-557. 10.1101/gad.1614408.

63. Montgomery, R.L., Davis, C.A., Potthoff, M.J., Haberland, M., Fielitz, J., Qi, X., Hill, J.A., Richardson, J.A., and Olson, E.N. (2007). Histone deacetylases 1 and 2 redundantly regulate cardiac morphogenesis, growth, and contractility. Genes Dev *21*, 1790-1802. 10.1101/gad.1563807.

64. Stuart, T., Butler, A., Hoffman, P., Hafemeister, C., Papalexi, E., Mauck, W.M., 3rd, Hao, Y., Stoeckius, M., Smibert, P., and Satija, R. (2019). Comprehensive Integration of Single-Cell Data. Cell *177*, 1888-1902 e1821. 10.1016/j.cell.2019.05.031.

65. La Manno, G., Soldatov, R., Zeisel, A., Braun, E., Hochgerner, H., Petukhov, V., Lidschreiber, K., Kastriti, M.E., Lonnerberg, P., Furlan, A., et al. (2018). RNA velocity of single cells. Nature *560*, 494-498. 10.1038/s41586-018-0414-6.

66. Li, S., Zhang, P., Chen, W., Ye, L., Brannan, K.W., Le, N.T., Abe, J.I., Cooke, J.P., and Wang, G. (2024). A relay velocity model infers cell-dependent RNA velocity. Nat Biotechnol *42*, 99-108. 10.1038/s41587-023-01728-5.

67. Robinson, M.D., McCarthy, D.J., and Smyth, G.K. (2010). edgeR: a Bioconductor package for differential expression analysis of digital gene expression data. Bioinformatics *26*, 139-140. 10.1093/bioinformatics/btp616.

68. Wu, T., Hu, E., Xu, S., Chen, M., Guo, P., Dai, Z., Feng, T., Zhou, L., Tang, W., Zhan, L., et al. (2021). clusterProfiler 4.0: A universal enrichment tool for interpreting omics data. Innovation (Camb) *2*, 100141. 10.1016/j.xinn.2021.100141.

69. Shannon, P., Markiel, A., Ozier, O., Baliga, N.S., Wang, J.T., Ramage, D., Amin, N., Schwikowski, B., and Ideker, T. (2003). Cytoscape: a software environment for integrated models of biomolecular interaction networks. Genome Res *13*, 2498-2504. 10.1101/gr.1239303.

70. Patro, R., Duggal, G., Love, M.I., Irizarry, R.A., and Kingsford, C. (2017). Salmon provides fast and bias-aware quantification of transcript expression. Nat Methods *14*, 417-419. 10.1038/nmeth.4197.

71. Love, M.I., Soneson, C., Hickey, P.F., Johnson, L.K., Pierce, N.T., Shepherd, L., Morgan, M., and Patro, R. (2020). Tximeta: Reference sequence checksums for provenance identification in RNA-seq. PLoS Comput Biol *16*, e1007664. 10.1371/journal.pcbi.1007664.

72. Durinck, S., Spellman, P.T., Birney, E., and Huber, W. (2009). Mapping identifiers for the integration of genomic datasets with the R/Bioconductor package biomaRt. Nat Protoc *4*, 1184-1191. 10.1038/nprot.2009.97.

73. Love, M.I., Huber, W., and Anders, S. (2014). Moderated estimation of fold change and dispersion for RNA-seq data with DESeq2. Genome Biol *15*, 550. 10.1186/s13059-014-0550-8.

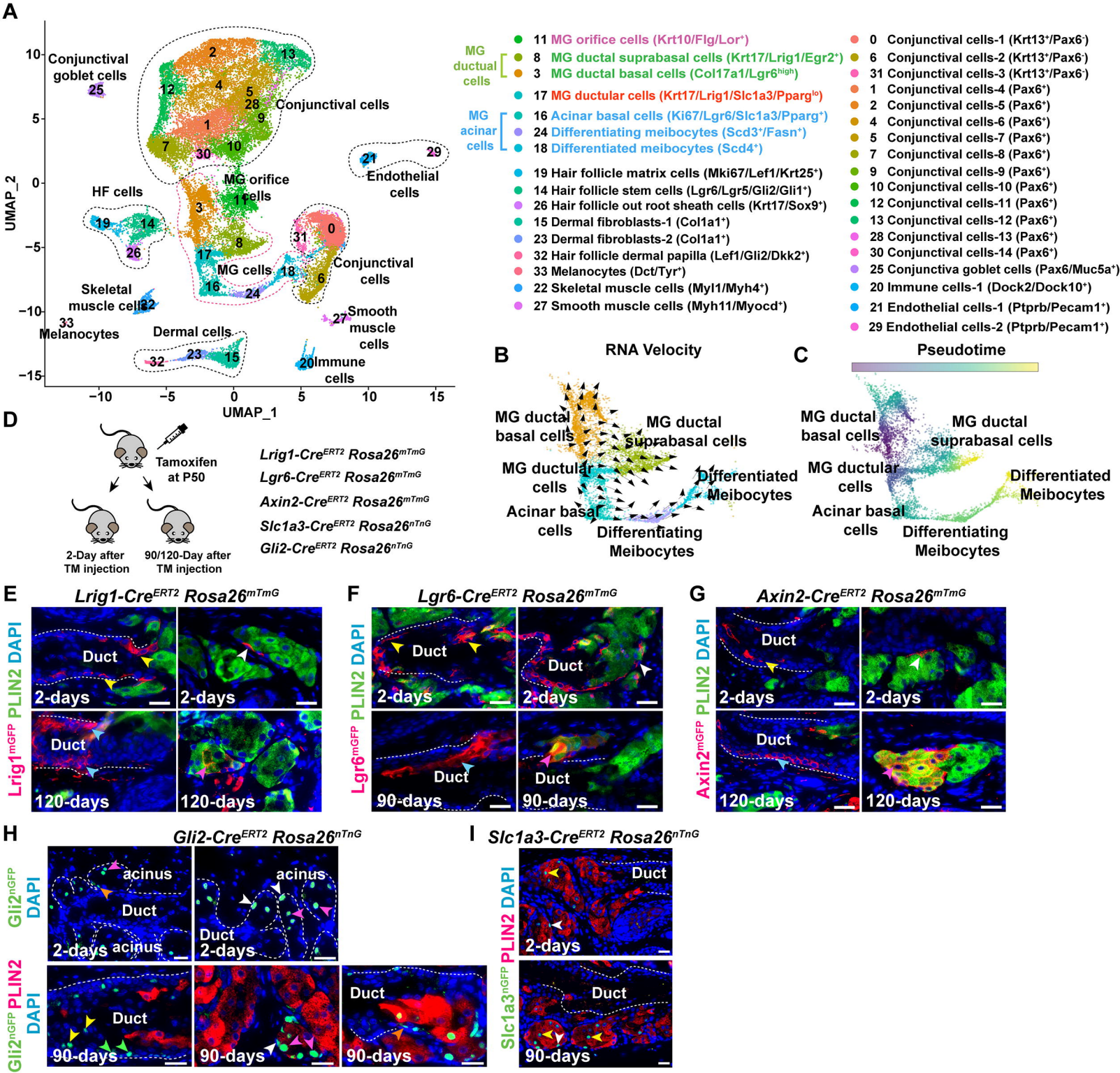
A
Conjunctival goblet cells
Conjunctival cells
MG orifice cells
HF cells
Endothelial cells
MG cells
Conjunctival cells
Skeletal muscle cells
Smooth muscle cells
Melanocytes
Dermal cells
Immune cells
UMAP_1
UMAP_2
MG ductual cells
MG acinar cells
11 MG orifice cells (Krt10/Flg/Lor+)
8 MG ductal suprabasal cells (Krt17/Lrig1/Egr2+)
3 MG ductal basal cells (Col17a1/Lgr6high)
17 MG ductular cells (Krt17/Lrig1/Slc1a3/Pparglo)
16 Acinar basal cells (Ki67/Lgr6/Slc1a3/Pparg+)
24 Differentiating meibocytes (Scd3+/Fasn+)
18 Differentiated meibocytes (Scd4+)
19 Hair follicle matrix cells (Mki67/Lef1/Krt25+)
14 Hair follicle stem cells (Lgr6/Lgr5/Gli2/Gli1+)
26 Hair follicle out root sheath cells (Krt17/Sox9+)
15 Dermal fibroblasts-1 (Col1a1+)
23 Dermal fibroblasts-2 (Col1a1+)
32 Hair follicle dermal papilla (Lef1/Gli2/Dkk2+)
33 Melanocytes (Dct/Tyr+)
22 Skeletal muscle cells (Myl1/Myh4+)
27 Smooth muscle cells (Myh11/Myocd+)
0 Conjunctival cells-1 (Krt13+/Pax6-)
6 Conjunctival cells-2 (Krt13+/Pax6-)
31 Conjunctival cells-3 (Krt13+/Pax6-)
1 Conjunctival cells-4 (Pax6+)
2 Conjunctival cells-5 (Pax6+)
4 Conjunctival cells-6 (Pax6+)
5 Conjunctival cells-7 (Pax6+)
7 Conjunctival cells-8 (Pax6+)
9 Conjunctival cells-9 (Pax6+)
10 Conjunctival cells-10 (Pax6+)
12 Conjunctival cells-11 (Pax6+)
13 Conjunctival cells-12 (Pax6+)
28 Conjunctival cells-13 (Pax6+)
30 Conjunctival cells-14 (Pax6+)
25 Conjunctiva goblet cells (Pax6/Muc5a+)
20 Immune cells-1 (Dock2/Dock10+)
21 Endothelial cells-1 (Ptprb/Pecam1+)
29 Endothelial cells-2 (Ptprb/Pecam1+)
B
RNA Velocity
MG ductal basal cells
MG ductal suprabasal cells
MG ductular cells
Differentiated Meibocytes
Acinar basal cells
Differentiating Meibocytes
C
Pseudotime
MG ductal basal cells
MG ductal suprabasal cells
MG ductular cells
Differentiated Meibocytes
Acinar basal cells
Differentiating Meibocytes
D
Tamoxifen at P50
2-Day after TM injection
90/120-Day after TM injection
Lrig1-CreERT2 Rosa26mTmG
Lgr6-CreERT2 Rosa26mTmG
Axin2-CreERT2 Rosa26mTmG
Slc1a3-CreERT2 Rosa26nTnG
Gli2-CreERT2 Rosa26nTnG
E
Lrig1-CreERT2 Rosa26mTmG
Lrig1mGFP PLIN2 DAPI
Duct
2-days
120-days
F
Lgr6-CreERT2 Rosa26mTmG
Lgr6mGFP PLIN2 DAPI
Duct
2-days
90-days
G
Axin2-CreERT2 Rosa26mTmG
Axin2mGFP PLIN2 DAPI
Duct
2-days
120-days
H
Gli2-CreERT2 Rosa26nTnG
Gli2nGFP DAPI
Gli2nGFP PLIN2 DAPI
acinus
Duct
2-days
90-days
I
Slc1a3-CreERT2 Rosa26nTnG
PLIN2 DAPI
Slc1a3nGFP
Duct
2-days
90-days

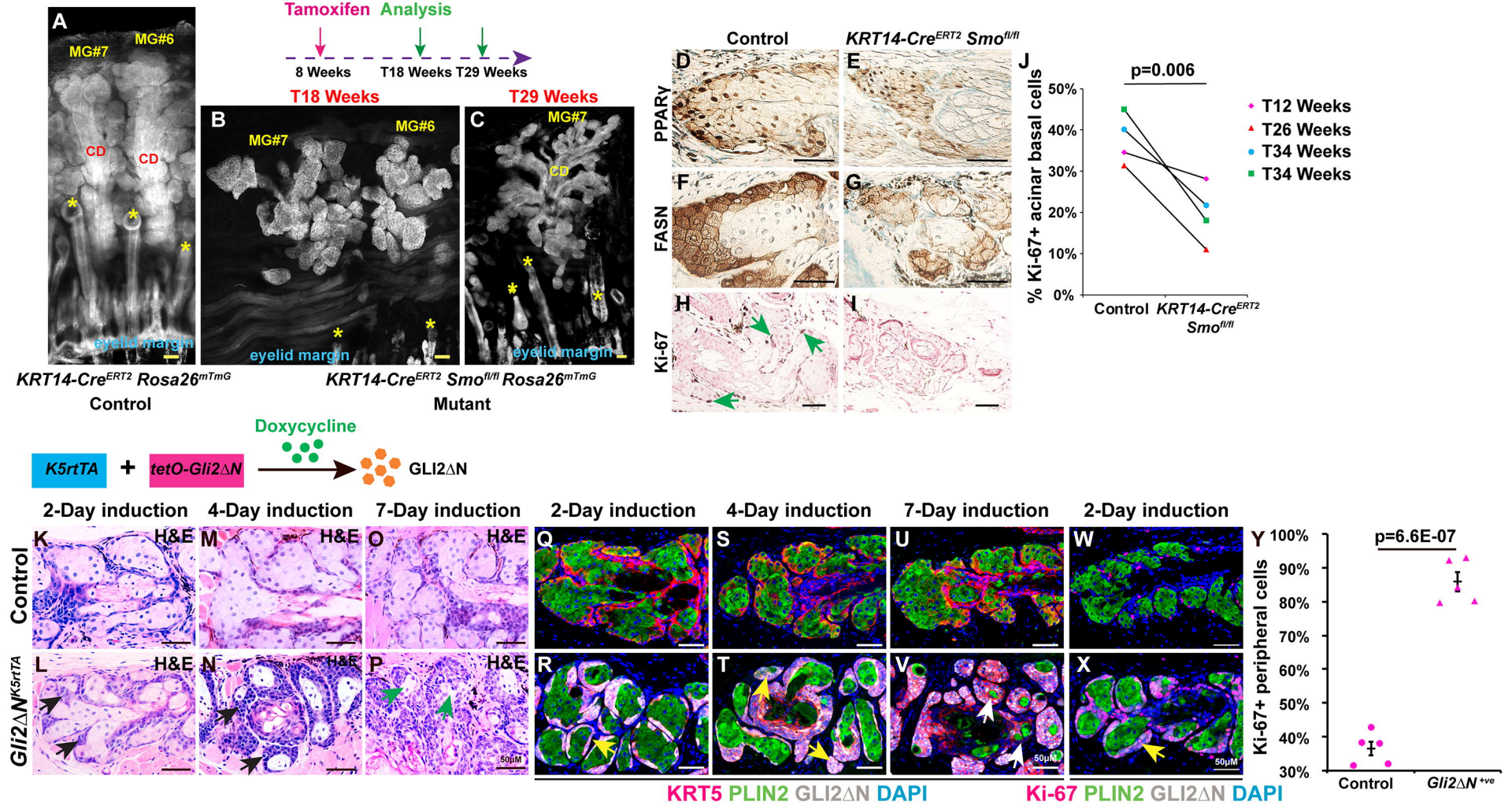
A
MG#7
MG#6
CD
CD
eyelid margin
Tamoxifen
Analysis
8 Weeks
T18 Weeks
T29 Weeks
T18 Weeks
T29 Weeks
B
MG#7
MG#6
eyelid margin
C
MG#7
CD
eyelid margin
KRT14-Cre^ERT2 Rosa26^mTmG
Control
KRT14-Cre^ERT2 Smo^fl/fl Rosa26^mTmG
Mutant
Control
KRT14-Cre^ERT2 Smo^fl/fl
D
E
PPARγ
F
G
FASN
H
I
Ki-67
J
p=0.006
% Ki-67+ acinar basal cells
50%
40%
30%
20%
10%
0%
Control
KRT14-Cre^ERT2 Smo^fl/fl
T12 Weeks
T26 Weeks
T34 Weeks
T34 Weeks
K5rtTA
+
tetO-Gli2ΔN
Doxycycline
GLI2ΔN
2-Day induction
4-Day induction
7-Day induction
2-Day induction
4-Day induction
7-Day induction
2-Day induction
Control
Gli2ΔN^K5rtTA
K
H&E
M
H&E
O
H&E
L
H&E
N
H&E
P
H&E
50μM
Q
S
U
W
R
T
V
50μM
X
50μM
KRT5 PLIN2 GLI2ΔN DAPI
Ki-67 PLIN2 GLI2ΔN DAPI
Y
p=6.6E-07
Ki-67+ peripheral cells
100%
90%
80%
70%
60%
50%
40%
30%
Control
Gli2ΔN^+ve

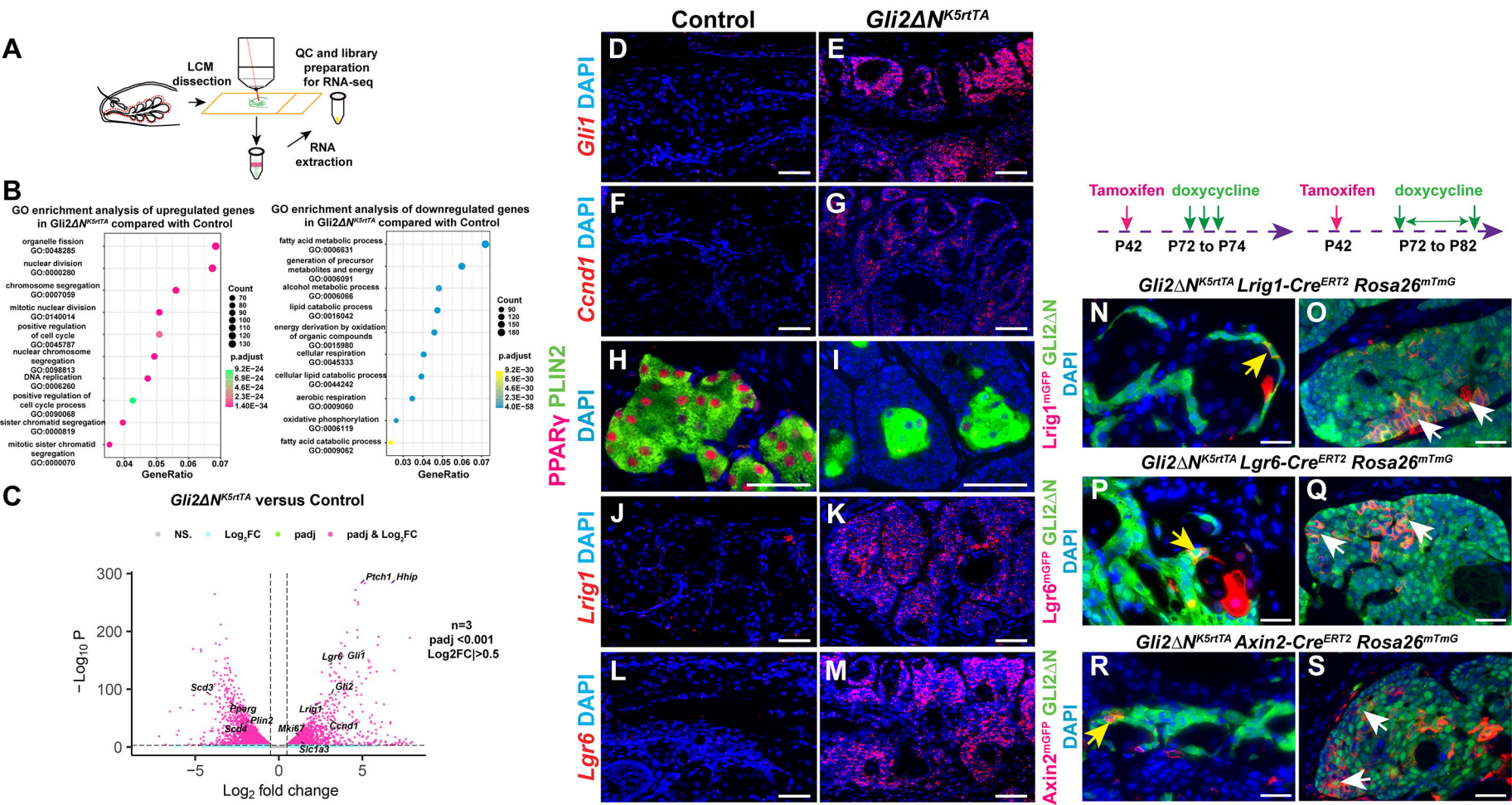
A
LCM dissection
QC and library preparation for RNA-seq
RNA extraction
B
GO enrichment analysis of upregulated genes in Gli2ΔN^K5rtTA compared with Control
organelle fission GO:0048285
nuclear division GO:0000280
chromosome segregation GO:0007059
mitotic nuclear division GO:0140014
positive regulation of cell cycle GO:0045787
nuclear chromosome segregation GO:0098813
DNA replication GO:0006260
positive regulation of cell cycle process GO:0090068
sister chromatid segregation GO:0000819
mitotic sister chromatid segregation GO:0000070
GeneRatio
Count
p.adjust
GO enrichment analysis of downregulated genes in Gli2ΔN^K5rtTA compared with Control
fatty acid metabolic process GO:0006631
generation of precursor metabolites and energy GO:0006091
alcohol metabolic process GO:0006066
lipid catabolic process GO:0016042
energy derivation by oxidation of organic compounds GO:0015980
cellular respiration GO:0045333
cellular lipid catabolic process GO:0044242
aerobic respiration GO:0009060
oxidative phosphorylation GO:0006119
fatty acid catabolic process GO:0009062
C
Gli2ΔN^K5rtTA versus Control
NS.
Log2FC
padj
padj & Log2FC
n=3
padj <0.001
Log2FC|>0.5
Ptch1 Hhip
Lgr6 Gli1
Gli2
Lrig1
Cchd1
Slc1a3
Mki67
Pparg
Plin2
Scd4
Scd3
− Log10 P
Log2 fold change
Control
Gli2ΔN^K5rtTA
Gli1 DAPI
Ccnd1 DAPI
PPARγ PLIN2 DAPI
Lrig1 DAPI
Lgr6 DAPI
Tamoxifen
doxycycline
P42
P72 to P74
P42
P72 to P82
Gli2ΔN^K5rtTA Lrig1-CreERT2 Rosa26mTmG
Lrig1mGFP GLI2ΔN DAPI
Gli2ΔN^K5rtTA Lgr6-CreERT2 Rosa26mTmG
Lgr6mGFP GLI2ΔN DAPI
Gli2ΔN^K5rtTA Axin2-CreERT2 Rosa26mTmG
Axin2mGFP GLI2ΔN DAPI

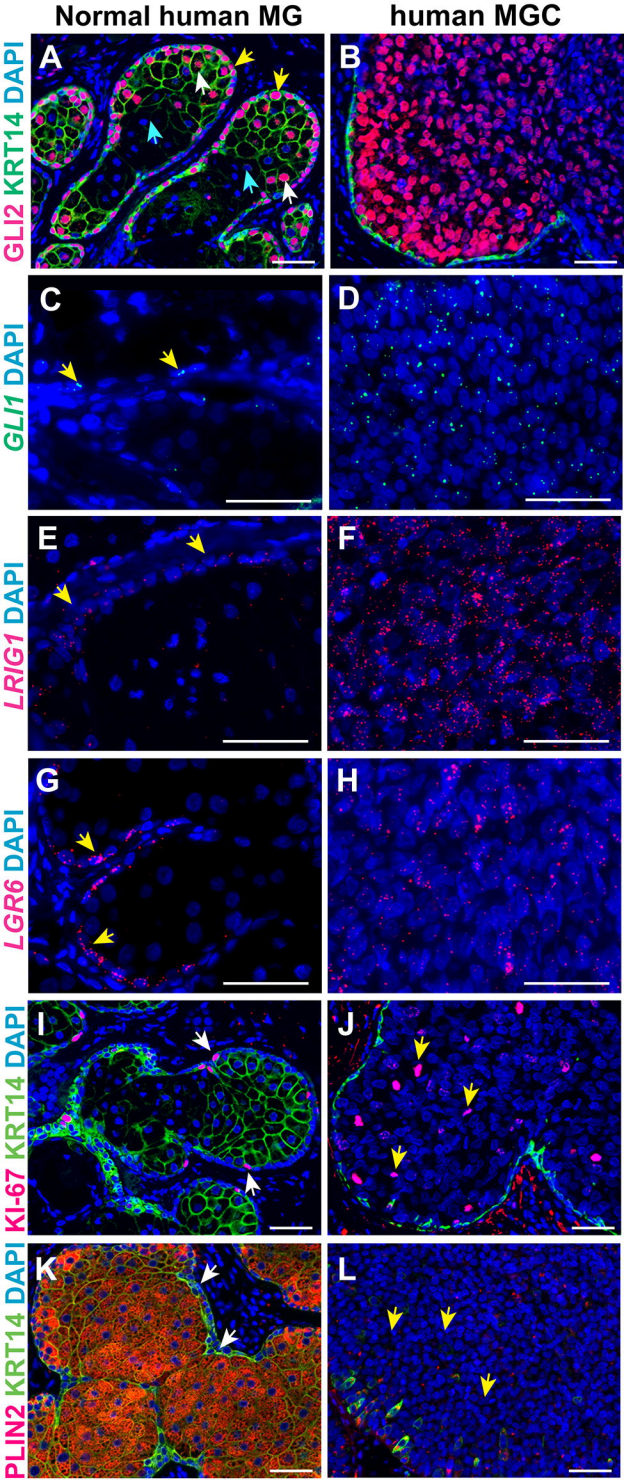
Normal human MG
human MGC
A
B
GLI2 KRT14 DAPI
C
D
GLI1 DAPI
E
F
LRIG1 DAPI
G
H
LGR6 DAPI
I
J
KI-67 KRT14 DAPI
K
L
PLIN2 KRT14 DAPI

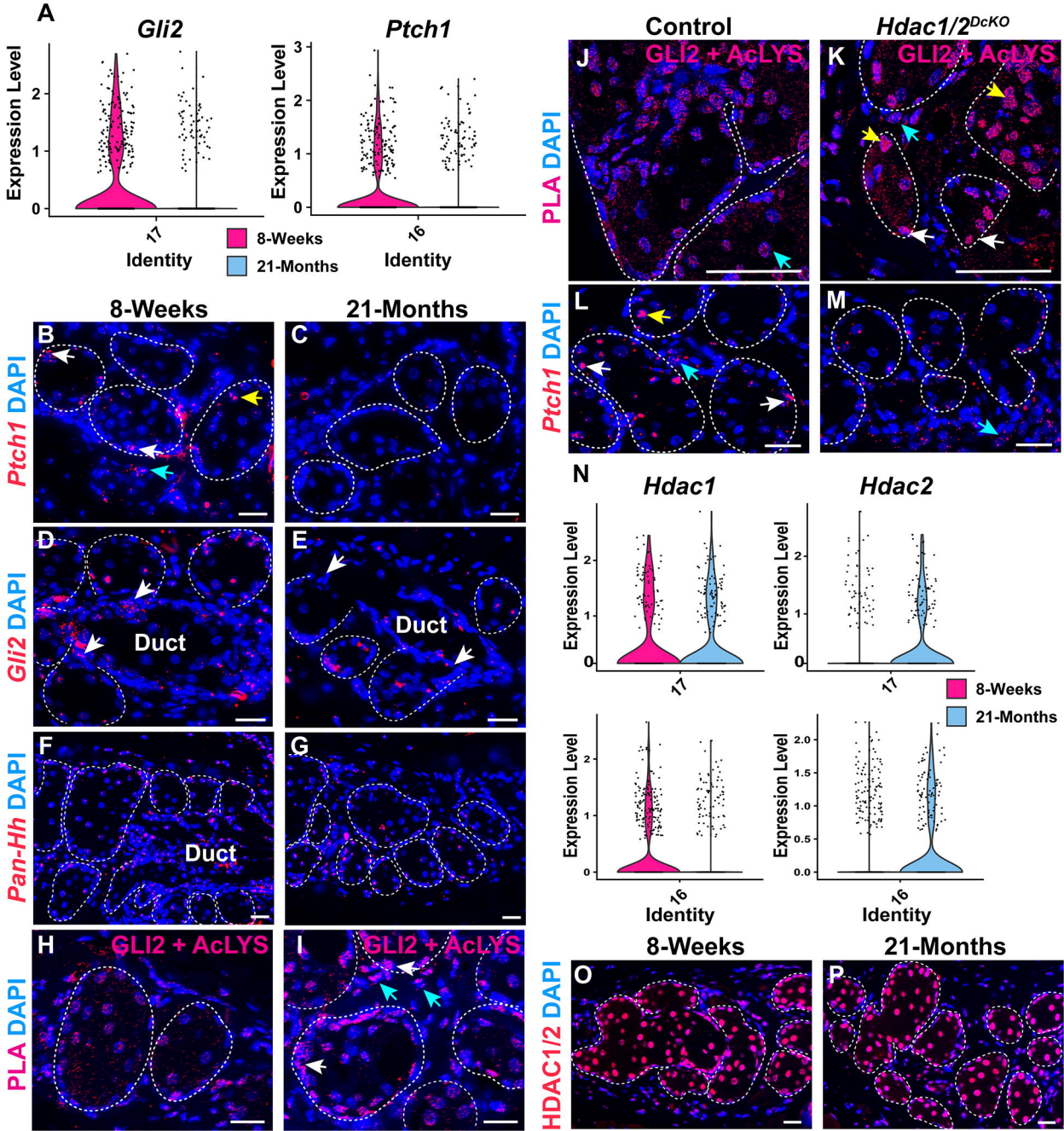
A
Gli2
Ptch1
Expression Level
Identity
8-Weeks
21-Months
Control
Hdac1/2DcKO
GLI2 + AcLYS
PLA DAPI
Ptch1 DAPI
Gli2 DAPI
Pan-Hh DAPI
HDAC1/2 DAPI
Duct
N
Hdac1
Hdac2

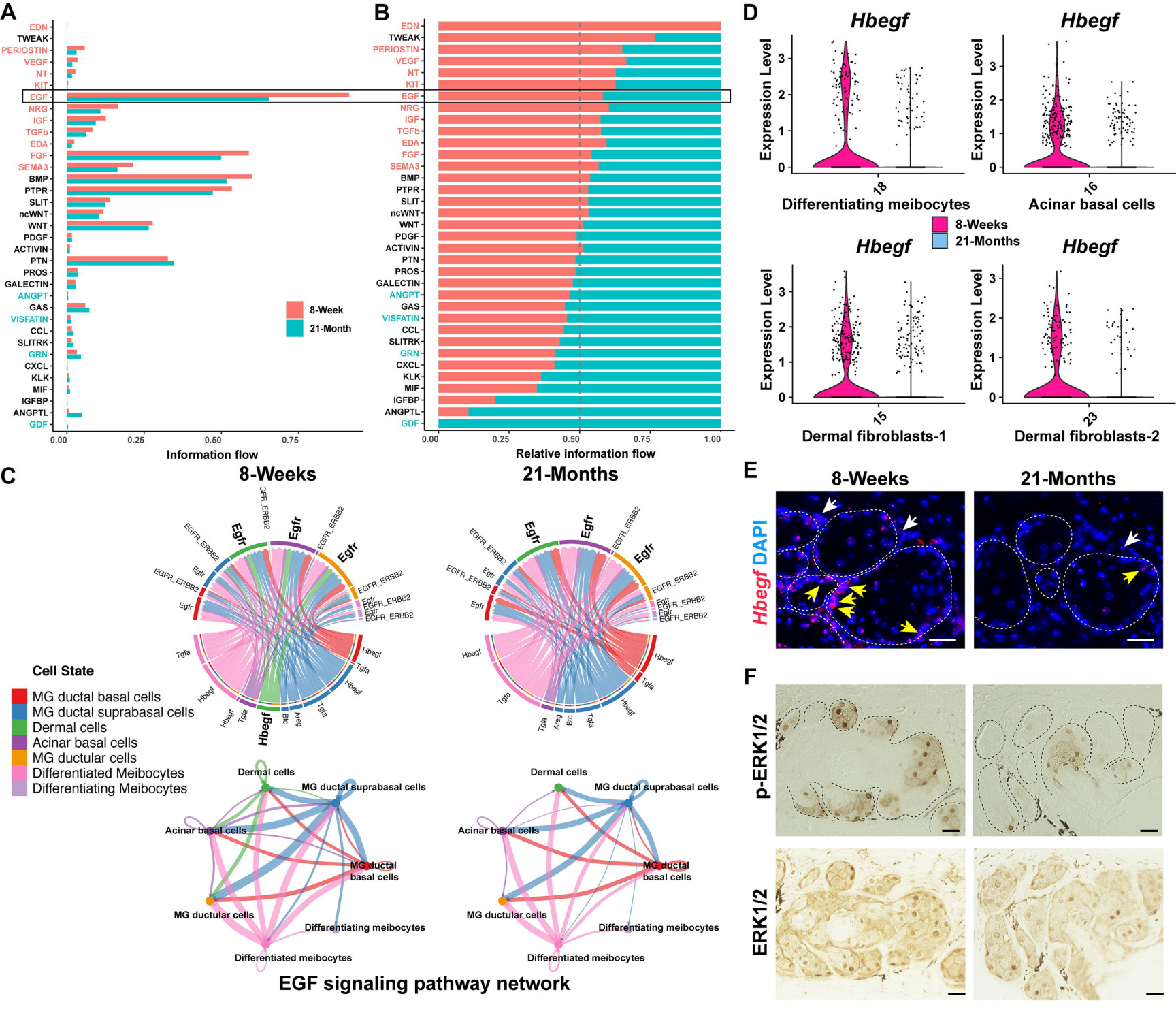
A
B
EDN
TWEAK
PERIOSTIN
VEGF
NT
KIT
EGF
NRG
IGF
TGFb
EDA
FGF
SEMA3
BMP
PTPR
SLIT
ncWNT
WNT
PDGF
ACTIVIN
PTN
PROS
GALECTIN
ANGPT
GAS
VISFATIN
CCL
SLITRK
GRN
CXCL
KLK
MIF
IGFBP
ANGPTL
GDF
8-Week
21-Month
Information flow
Relative information flow
D
Hbegf
Expression Level
Differentiating meibocytes
Acinar basal cells
8-Weeks
21-Months
Dermal fibroblasts-1
Dermal fibroblasts-2
C
8-Weeks
21-Months
Cell State
MG ductal basal cells
MG ductal suprabasal cells
Dermal cells
Acinar basal cells
MG ductular cells
Differentiated Meibocytes
Differentiating Meibocytes
MG ductal basal cells
Differentiating meibocytes
Differentiated meibocytes
EGF signaling pathway network
E
8-Weeks
21-Months
Hbegf DAPI
F
p-ERK1/2
ERK1/2

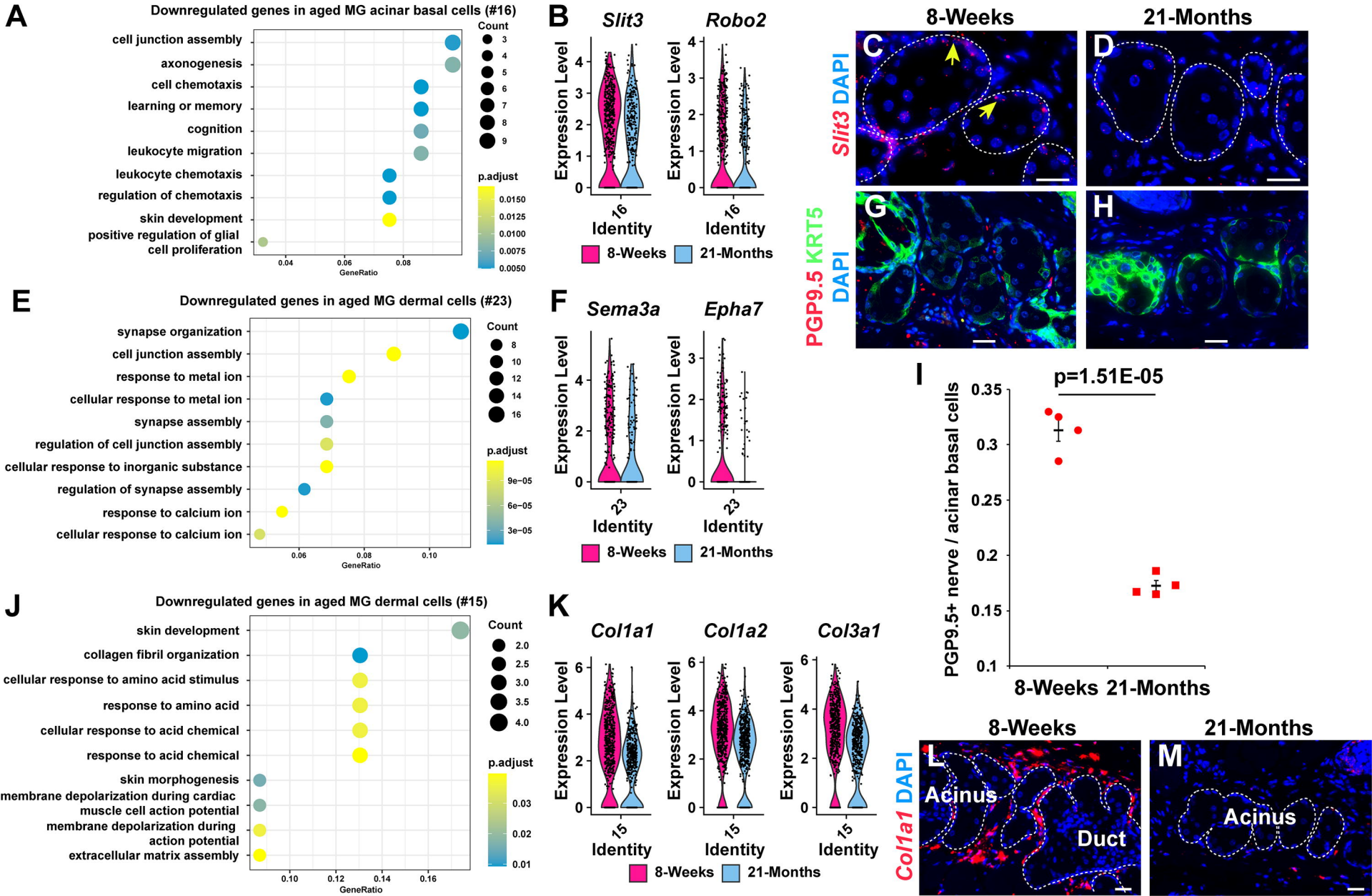
A
Downregulated genes in aged MG acinar basal cells (#16)
cell junction assembly
axonogenesis
cell chemotaxis
learning or memory
cognition
leukocyte migration
leukocyte chemotaxis
regulation of chemotaxis
skin development
positive regulation of glial cell proliferation
0.04
0.06
0.08
GeneRatio
Count
3
4
5
6
7
8
9
p.adjust
0.0150
0.0125
0.0100
0.0075
0.0050
B
Slit3
Robo2
Expression Level
16
Identity
8-Weeks
21-Months
8-Weeks
21-Months
C
D
Slit3 DAPI
G
H
PGP9.5 KRT5 DAPI
E
Downregulated genes in aged MG dermal cells (#23)
synapse organization
cell junction assembly
response to metal ion
cellular response to metal ion
synapse assembly
regulation of cell junction assembly
cellular response to inorganic substance
regulation of synapse assembly
response to calcium ion
cellular response to calcium ion
0.06
0.08
0.10
GeneRatio
Count
8
10
12
14
16
p.adjust
9e−05
6e−05
3e−05
F
Sema3a
Epha7
Expression Level
23
Identity
8-Weeks
21-Months
I
p=1.51E-05
PGP9.5+ nerve / acinar basal cells
0.35
0.3
0.25
0.2
0.15
0.1
8-Weeks
21-Months
J
Downregulated genes in aged MG dermal cells (#15)
skin development
collagen fibril organization
cellular response to amino acid stimulus
response to amino acid
cellular response to acid chemical
response to acid chemical
skin morphogenesis
membrane depolarization during cardiac muscle cell action potential
membrane depolarization during action potential
extracellular matrix assembly
0.10
0.12
0.14
0.16
GeneRatio
Count
2.0
2.5
3.0
3.5
4.0
p.adjust
0.03
0.02
0.01
K
Col1a1
Col1a2
Col3a1
Expression Level
15
Identity
8-Weeks
21-Months
8-Weeks
21-Months
L
Acinus
Duct
M
Acinus
Col1a1 DAPI

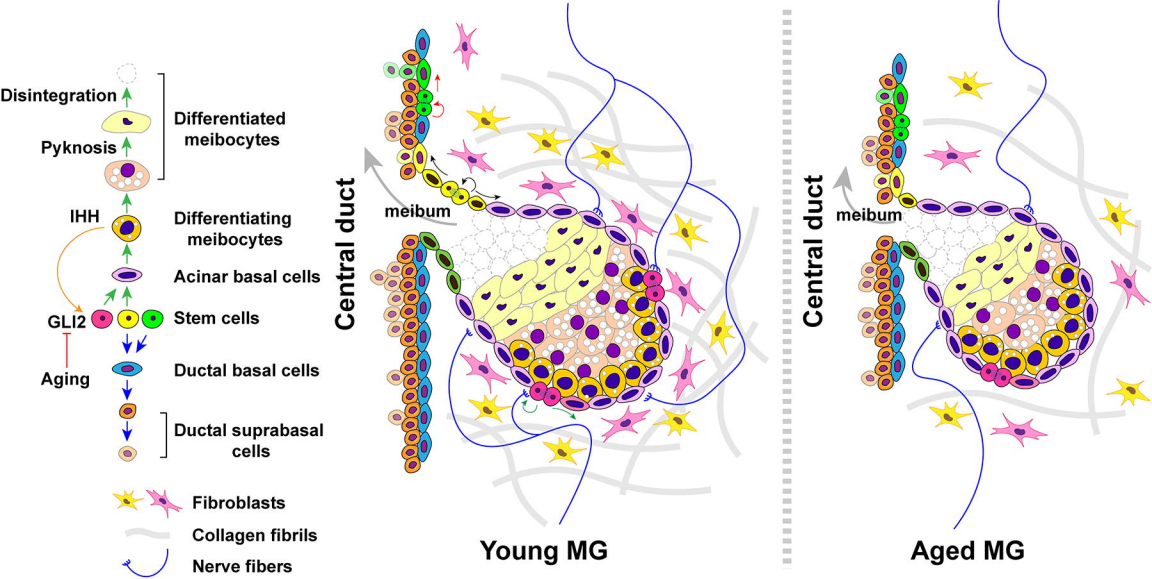
Disintegration
Pyknosis
Differentiated meibocytes
IHH
Differentiating meibocytes
Acinar basal cells
GLI2
Stem cells
Aging
Ductal basal cells
Ductal suprabasal cells
Fibroblasts
Collagen fibrils
Nerve fibers
Central duct
meibum
Young MG
Central duct
meibum
Aged MG